LANGMUIR

pubs.acs.org/Langmuir Article

Conformal Sites Theory for Adsorbed Films on Energetically Heterogeneous Surfaces

Kaihang Shi, Erik E. Santiso,* and Keith E. Gubbins*

Cite This: https://dx.doi.org/10.1021/acs.langmuir.9b03633 Read Online

ACCESS | Metrics & More | Article Recommendations

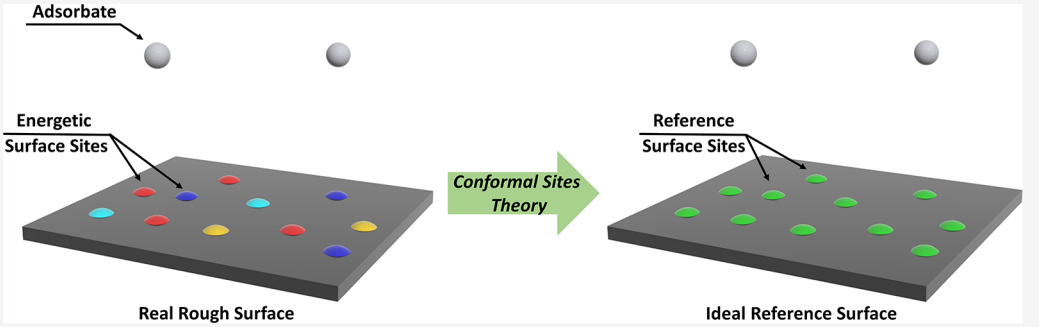

ABSTRACT: We present a conformal sites theory for a solid substrate whose surface is both geometrically and energetically heterogeneous and that interacts with an adsorbed film. The theory is based on a perturbation expansion for the grand potential of a real system with a rough surface about that of a reference system with an ideal reference surface, thus mapping the real system onto a much simpler interfacial system. The expansion is in powers of the intermolecular potential parameters, and leads to mixing rules for the potential parameters of the reference system. Grand canonical Monte Carlo simulations for the adsorption of argon at 87.3 K, carbon dioxide at 273 K, and water vapor at 298 K on heterogeneous carbon surfaces are investigated to explore the limits of applicability of the theory. Simulation results indicate that the theory works well with typical asymmetry of the potential parameters in the force field. However, care should be taken when applying the theory to strongly associating fluids and in the low-pressure region where the active surface sites play an important role. The conformal sites theory can be used to predict the adsorption properties and to characterize the solid substrate by taking advantage of the corresponding states principle. Other possible applications are also discussed.

1. INTRODUCTION

Molecular simulation and theoretical treatments of thin films adsorbed onto solid surfaces or within narrow pores have usually treated the solid surface as atomically smooth and energetically homogeneous. Thus, while nonlocal density functional theory (NLDFT)[1−4] greatly improves the determination of pore size distribution (PSD) of activated carbons, early versions of the theory assumed that the graphite surface is smooth, uncorrugated, and chemically homogeneous; this results in errors in the determination of the PSD.[5,6] In practice, nearly all surfaces exhibit roughness through geometric effects (e.g., curvature of graphene segments due to defects) and variations in chemical composition or chemical groups attached to the surfaces. Such surface roughness is known to be important for adsorption at a low bulk pressure[5,7] during the completion of the first adsorbed layer for the pressure tensor in thin films[8] and phase transitions in pores, including freezing,[9−11] layering transitions,[5,12] and contact layer phases[13] for example. A variety of simple models have been proposed for geometrically and energetically heterogeneous surfaces at both the macro- and nanoscales. Nanoscale models have been reviewed by Jagiello and Olivier[5] recently. Included are models that account for geometric surface vacancies,[14,15] variable wall thickness,[16] or variable surface density[6,17] and also models that add a periodic function to the solid−fluid interaction potential in a direction parallel to the pore wall.[5,18,19] While the quenched solid density functional theory[6] and also the 2D-NLDFT[5] give good agreement with experimental low pressure adsorption data, they are limited in that they allow for only one kind of heterogeneity at a time (i.e., either structural or chemical heterogeneity). Jagiello and Olivier[20] have attempted to include both geometric and chemical effects into one comprehensive model; however, their model does not permit variation of the energetic site densities and fails to consider the electrostatic

Received: November 24, 2019
Published: January 27, 2020

interactions, which are of particular importance for the adsorption of polar molecules, for example, water and carbon dioxide, onto grafted or oxidized surfaces at a low pressure. In molecular simulations, it is possible to study the adsorption process based on a detailed model of surface roughness in slit pores[7,21,22] and cylindrical pores.[23] However, simple and accurate roughness models that can be incorporated into theoretical approaches, such as classical density functional theory[5,18,19] or corresponding states theory,[24,25] are more easily used by experimentalists for fast predictions.

In this work, we propose a simple statistical mechanical model of surface roughness that allows for an arbitrary number of types of surface sites and variable site densities. We consider the surface to be made up of a number of patches or sites of varying interaction energy. The key assumption made is that the interaction energy of these patches with an adsorbate molecule is conformal, that is, they conform to the same functional form. The approach is analogous to that of the van der Waals 1-fluid (vdW1) theory of simple, spherical molecules that has been very successful for the thermodynamic properties of simple bulk liquid mixtures.[26−32] The main limitations of these theories of liquid mixtures are their restriction to spherical, nonpolar molecules and liquids that are uniform in density. Here, we extend such treatments to systems where the molecules are nonspherical and exhibit electrostatic forces, and to highly inhomogeneous systems that include a substrate having an energetically and geometrically rough surface. Recently, An et al.[33] proposed a conformal sites analysis for the static and dynamic properties of polymer films on a homogeneous substrate. The model in this paper focuses specifically on elucidating the molecular-level factors responsible for the surface heterogeneity.

2. CONFORMAL SITES THEORY

In the spirit of the corresponding states theory,[24,25] perturbation theory,[28] and vdW1 theory,[26,27] we develop a statistical mechanical analysis, which we term the conformal sites theory, for the interfacial system involving nonspherical adsorbate molecules and rough surfaces.

We assume that the surface layer of the solid substrate is made up of different adsorption sites of species α, β, ..., which can include atoms (δ, e.g., carbon) that are the main constituents of the solid substrate and other energetic adsorption sites; the heterogeneous sites are assumed to be present only on the surface of the solid substrate. The adsorbate molecule interacts with atoms in the lower layers of the substrate in the same way as for the homogeneous substrate. For simplicity of notation, we assume that the homogeneous regions of the substrate are made up of $N_{\text{site}}^{\text{lower}}$ sites of only one atomic species, δ; however, the extension to multiple species of atom is straightforward. We consider the top surface having N_α surface sites of species α, N_β sites of species β, and so on, with varying interaction strengths. The total number of top surface sites is $N_{\text{site}}^{\text{top}} = \sum_\alpha N_\alpha$; these top surface sites, will in general, include δ sites. Thus, the total number of substrate sites is $N_{\text{site}} = N_{\text{site}}^{\text{top}} + N_{\text{site}}^{\text{lower}}$. We further assume a pure adsorbate phase and that each adsorbate molecule possesses m interaction sites of species κ, λ, ... The adsorbate−adsorbate and adsorbate−substrate interaction potentials are taken to be pair-wise additive and include terms for overlap, dispersion, and electrostatic forces in general. Thus, the adsorbate−adsorbate (aa) interactions are of the form

$$U_{\text{aa}} = \sum_i \sum_j \sum_\upsilon \sum_\xi u_{ij}^{\text{a-a}}(r_{\upsilon\xi}) \tag{1}$$

where $u_{ij}^{\text{a-a}}(r_{\upsilon\xi})$ is the adsorbate−adsorbate intermolecular potential energy between site υ in adsorbate molecule i and site ξ in adsorbate molecule j and is of the form

$$u_{ij}^{\text{a-a}}(r_{\upsilon\xi}) = \varepsilon_{\upsilon\xi} f\left(\frac{r_{\upsilon\xi}}{\sigma_{\upsilon\xi}}\right) + \frac{q_\upsilon q_\xi}{4\pi\varepsilon_0 r_{\upsilon\xi}} \tag{2}$$

where $\varepsilon_{\upsilon\xi}$ and $\sigma_{\upsilon\xi}$ are potential parameters having units of energy and distance, respectively, q_υ is a point charge on site υ, ε_0 is the permittivity of vacuum, and $r_{\upsilon\xi}$ is the separation between site υ and site ξ. The first term on the right of eq 2 accounts for dispersion and overlap forces, the form of which is taken to be of 12-6 Lennard-Jones (LJ) form[34] in this work, while the second accounts for Coulombic forces. Nonbonded potentials of the form of eq 2 have been used for a wide range of nonpolar, polar, and associating molecules, with parameter values fitted to *ab initio* and experimental data; examples include the TIP,[35] OPLS,[36] and CHARMM[37] force fields. It is worth noting that some site−site interactions will involve only the LJ interaction, some will involve only the Coulombic interaction, and some will involve both.

We are interested in calculating the free energy of adsorption. We treat the adsorbate molecules as being, in general, nonspherical but rigid. The adsorbed phase is open to exchange of molecules with the bulk reservoir (i.e., the number of adsorbate molecules N_a is fluctuating), but the numbers of atoms and sites in the substrate are fixed. We therefore adopt a semigrand canonical ensemble,[38−41] which is characterized by the variables N_α, N_β, ... $\equiv \{N_\alpha\}$ (number of substrate sites of various species), μ_a (chemical potential of adsorbate molecules), V (accessible volume of the system), and T (temperature). Let $U(\mathbf{R}^{\{N_\alpha\}}, \mathbf{r}^{N_a}, \omega^{N_a})$ be the total configurational energy, including the contributions from adsorbate−adsorbate and adsorbate−substrate interactions. Here, we have assumed the substrate sites to be fixed, and $\mathbf{R}^{\{N_\alpha\}}$ represents the positions of substrate sites. The semigrand partition function of the interfacial system for a given substrate configuration $\mathbf{R}^{\{N_\alpha\}}$ is[38−41]

$$\Xi(\mu_a, \{N_\alpha\}, V, T) = \sum_{N_a=0}^{\infty} \frac{z_a^{N_a}}{N_a!} \times \int \exp[-U(\mathbf{R}^{\{N_\alpha\}}, \mathbf{r}^{N_a}, \omega^{N_a})/k_B T]\, \mathrm{d}\mathbf{r}^{N_a}\, \mathrm{d}\omega^{N_a} \tag{3}$$

where k_B is the Boltzmann constant, and $\mathbf{r}^{N_a} \equiv \mathbf{r}_1, \mathbf{r}_2 ..., \mathbf{r}_{N_a}$ and $\omega^{N_a} \equiv \omega_1, \omega_2 ..., \omega_{N_a}$ represent the positions and orientations of all adsorbate molecules. The activity, z_a, of a single adsorbate molecule is

$$z_a = \frac{\exp(\mu_a/k_B T) q_{a,qu}}{\Lambda_{a,t}^3 \Lambda_{a,r} \bar{\omega}} \tag{4}$$

where $\Lambda_{a,t}$ is the translational part (de Broglie wavelength) and $\Lambda_{a,r}$ is the rotational part of the kinetic energy in the molecular partition function, $q_{a,qu}$ is the part that must be treated quantally, and $\bar{\omega} = \int \mathrm{d}\omega$, that is, 4π or $8\pi^2$ for linear or nonlinear molecules, respectively. The total configurational energy $U(\mathbf{R}^{\{N_\alpha\}}, \mathbf{r}^{N_a}, \omega^{N_a})$ in eq 3 can be written as

https://dx.doi.org/10.1021/acs.langmuir.9b03633
Langmuir XXXX, XXX, XXX−XXX

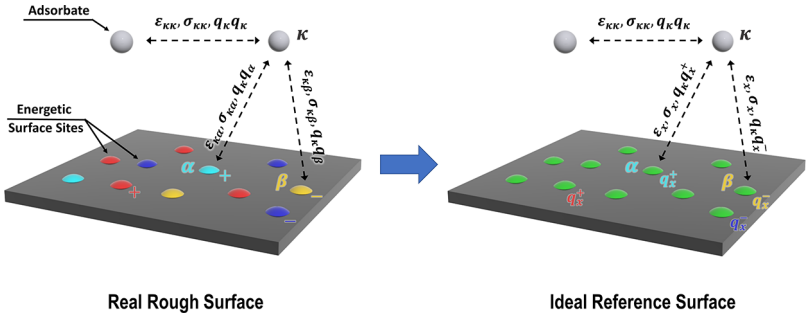

Figure 1. Schematic plot of the conformal sites theory mapping from a real system (left) to a reference system (right). Left: the energetically heterogeneous surface with four types of energetic site (indicated by different colors), among which the α sites (cyan spherical cap) and the β sites (yellow spherical cap) are labeled as examples. α sites carry positive charges and have interaction parameters $\varepsilon_{\kappa\alpha}$, $\sigma_{\kappa\alpha}$, and $q_\kappa q_\alpha$ with adsorbate site κ (gray adsorbate molecule); β sites carry negative charges and have parameters $\varepsilon_{\kappa\beta}$, $\sigma_{\kappa\beta}$, and $q_\kappa q_\beta$ with adsorbate site κ. Right: the ideal reference surface, where all energetic sites are colored in green to indicate that they are conformal reference sites and interact with the adsorbate molecule κ with the same Lennard-Jones potential parameters ε_x and σ_x. By construction, the number, position, and identity of charged sites on the reference surface remain the same as those on the real rough surface but with the reference charges of q_x^+ for positive surface charges and q_x^- for negative surface charges. For example, α sites and β sites on the reference surface now interact with adsorbate site κ with parameters of $q_\kappa q_x^+$ and $q_\kappa q_x^-$, respectively. The primary substrate atoms δ are not shown for clarity.

$$
\begin{aligned}
U(\mathbf{R}^{\{N_\alpha\}}, \mathbf{r}^{N_a}, \omega^{N_a}) &= \sum_i \sum_j \sum_\upsilon \sum_\xi u_{ij}^{a-a}(r_{\upsilon\xi}) \\
&+ \sum_i \sum_\upsilon \sum_l u^{a-top}(r_{\upsilon l}) + \sum_i \sum_\upsilon \sum_l u^{a-lower}(r_{\upsilon l}) \\
&= \sum_i \sum_j \sum_\upsilon \sum_\xi \left[\varepsilon_{\upsilon\xi} f\left(\frac{r_{\upsilon\xi}}{\sigma_{\upsilon\xi}}\right) + \frac{q_\upsilon q_\xi}{4\pi\varepsilon_0 r_{\upsilon\xi}} \right] \\
&+ \sum_i \sum_\upsilon \sum_l \left[\varepsilon_{\upsilon l} f\left(\frac{r_{\upsilon l}}{\sigma_{\upsilon l}}\right) + \frac{q_\upsilon q_l}{4\pi\varepsilon_0 r_{\upsilon l}} \right] \\
&+ \sum_i \sum_\upsilon \sum_l \varepsilon_{\upsilon l} f\left(\frac{r_{\upsilon l}}{\sigma_{\upsilon l}}\right)
\end{aligned}
\tag{5}
$$

The first term on the right of eq 5 is the sum of all adsorbate−adsorbate interactions. The second term on the right is the sum of all interactions between the site υ in adsorbate molecule i and a top surface site l, and the final term on the right is the contribution of interactions between site υ in adsorbate molecule i and the lower layer substrate site l. We have assumed that the δ atoms (the main component of the substrate) do not carry electrostatic charges. We also have neglected the interactions between pairs of substrate sites since we consider these sites to be fixed. The semigrand potential thus is[40]

$$
\Omega(\mu_a, \{N_\alpha\}, V, T) = -k_B T \ln \Xi(\mu_a, \{N_\alpha\}, V, T) \tag{6}
$$

We now map the semigrand potential for the real system with a rough surface, given by eq 6, to that for a reference system with an ideal reference surface having the same number of adsorption sites as the rough surface. For the reference system, the surface sites interact with the adsorbate sites with a potential form that is conformal with that for the α, β, ... sites on the rough surface but with all adsorbate−surface site−site dispersive interactions having the same potential parameters ε_x and σ_x, regardless of the site species, where subscript x indicates the reference system. In mapping the point charges on the real surface onto those on the reference surface, we require that the number, position, and identity of the reference charged sites remains the same as those on the real rough surface, with new reference point charges of q_x^+ and q_x^- for positively and negatively charged surface sites, respectively. We will show that such a construction can intrinsically maintain the electrical neutrality of the reference surface. This mapping process is illustrated in Figure 1; this process only changes the adsorbate−surface site−site cross-interaction parameters, and the identity of the surface/adsorbate site will remain the same as that in the original real system, which is similar to the vdW1 theory.[31] We note that, for the real heterogeneous surface, some surface sites will carry a point charge, while others may have only site−site LJ interactions.

To realize this mapping process, we wish to expand the semigrand potential for the real system about that for the reference system in powers of the difference in the adsorbate−surface pair potential parameters for the real system and the ideal reference system. We must first decide on the appropriate choice of expansion variables that gives the most rapid convergence of the corresponding Taylor expansion. In the conformal theory of liquid mixtures of spherical molecules (components α, β,...), several choices were proposed. In the original work of Longuet-Higgins,[42] the expansion was in terms of $(\varepsilon_{\alpha\beta} - \varepsilon_x)$ and $(\sigma_{\alpha\beta} - \sigma_x)$, whereas in the random mixture[43,44] version of the theory, $(\varepsilon_{\alpha\beta}\sigma_{\alpha\beta}^{12} - \varepsilon_x\sigma_x^{12})$ and $(\varepsilon_{\alpha\beta}\sigma_{\alpha\beta}^{6} - \varepsilon_x\sigma_x^{6})$ were used as the expansion variables. Leland and co-workers[26,27] used $(\varepsilon_{\alpha\beta}\sigma_{\alpha\beta}^{3} - \varepsilon_x\sigma_x^{3})$ and $(\sigma_{\alpha\beta}^{3} - \sigma_x^{3})$ as expansion variables, which yield the van der Waals one-fluid (vdW1) theory, so-called because the resulting mixing rules for ε_x and σ_x correspond to those used by van der Waals in his theory of mixtures; "one fluid" because the theory relates the properties of the mixture to those for a single reference pure fluid. Among these choices, the vdW1 choice gave, by far, the best agreement with the simulations.[30,45−49] That the vdW1 choice of expansion parameters is a reasonable one is also supported by examination of the equations for the internal energy and pressure for mixtures.[45,46] While the vdW1 expansion parameters were found to work well, this was for spherical Lennard-Jones interactions only. However, using similar arguments proposed by Henderson and Leonard,[45,46] it is possible to show that a similar choice is appropriate for molecules and surface sites that interact with site−site intermolecular potentials, as we show in Appendix A.1. We therefore adopt the vdW1 choice of expansion variables here, $(\varepsilon_{\kappa\alpha}\sigma_{\kappa\alpha}^{3} - \varepsilon_x\sigma_x^{3})$ and $(\sigma_{\kappa\alpha}^{3} - \sigma_x^{3})$, remembering κ is the site species in the adsorbate molecule and α is the site species on the rough surface. As far as we are aware, there have not been previous attempts to include the point charge terms in a conformal

https://dx.doi.org/10.1021/acs.langmuir.9b03633
Langmuir XXXX, XXX, XXX−XXX

solution treatment. Examination of the equation for the configuration energy for a fluid having such site−site electrostatic interactions suggests that using $(q_\alpha - q_x)$ as the expansion variable is appropriate (see Appendix A.2). The reference charge q_x here is a general notation, and it becomes q_x^+ and q_x^- when the surface charge q_α is positive and negative, respectively. The semigrand potential for the real system is then to the first order

$$\Omega = \Omega_x + \sum_\kappa^\dagger \sum_\alpha^\dagger \left(\frac{\partial\Omega}{\partial(\sigma_{\kappa\alpha}^3)}\right)_x (\sigma_{\kappa\alpha}^3 - \sigma_x^3) + \sum_\kappa^\dagger \sum_\alpha^\dagger \left(\frac{\partial\Omega}{\partial(\varepsilon_{\kappa\alpha}\sigma_{\kappa\alpha}^3)}\right)_x (\varepsilon_{\kappa\alpha}\sigma_{\kappa\alpha}^3 - \varepsilon_x\sigma_x^3) + \sum_\alpha^+ \left(\frac{\partial\Omega}{\partial(q_\alpha)}\right)_x (q_\alpha - q_x^+) + \sum_\alpha^- \left(\frac{\partial\Omega}{\partial(q_\alpha)}\right)_x \times (q_\alpha - q_x^-) + \text{second-order terms ...} \quad (7)$$

where subscript x signifies the limit when $\varepsilon_{\kappa\alpha} \to \varepsilon_x$, $\sigma_{\kappa\alpha} \to \sigma_x$, and $q_\alpha \to q_x^+$ (or q_x^-). The dagger on the summation signs indicate that the sum is over all adsorbate−surface site species pairs, none of which has zero size parameter (i.e., $\sigma_{\kappa\kappa}$, $\sigma_{\alpha\alpha} \neq 0$); and the summation over the top surface site species (α, β, ...) includes both primary substrate site species (δ) and energetic surface site species. For the fourth and fifth terms on the right of eq 7, $\sum_\alpha^+$and $\sum_\alpha^-$ indicate a summation over all surface site types with positive charge and all surface site types with negative charge, respectively.

We first consider the derivative with respect to $\sigma_{\kappa\alpha}^3$. We note that the only term in eq 5 that depends on $\sigma_{\kappa\alpha}^3$ is the second on the right. The number of possible $\kappa\alpha$ type pair interactions is $N_\kappa N_\alpha$. If we assume that the surface sites of type α share a similar chemical environment on the rough surface and the adsorbate sites of type κ are geometrically symmetric on the adsorbate molecule, each of these $\kappa\alpha$ type pair interactions will give similar results after the integration over the whole space. So, from eqs 3, 5, and 6, we find

$$\begin{aligned}\frac{\partial\Omega}{\partial\sigma_{\kappa\alpha}^3} &= -k_BT\frac{1}{\Xi}\frac{\partial\Xi}{\partial\sigma_{\kappa\alpha}^3} \\ &= -k_BT\frac{1}{\Xi}\left(\sum_{N_a=0}^{\infty}\frac{z_a^{N_a}}{N_a!}\int\frac{\partial(-U/k_BT)}{\partial(\sigma_{\kappa\alpha}^3)} \times \exp[-U(\mathbf{R}^{\{N_\alpha\}}, \mathbf{r}^{N_a}, \omega^{N_a})/k_BT]\, d\mathbf{r}^{N_a}\, d\omega^{N_a}\right) \\ &\approx \frac{N_\alpha}{\Xi}\left(\sum_{N_a=0}^{\infty}\frac{N_\kappa z_a^{N_a}}{N_a!}\int\frac{\partial}{\partial(\sigma_{\kappa\alpha}^3)}\left[\varepsilon_{\kappa\alpha}f\left(\frac{r_{\kappa\alpha}}{\sigma_{\kappa\alpha}}\right)\right] \times \exp[-U(\mathbf{R}^{\{N_\alpha\}}, \mathbf{r}^{N_a}, \omega^{N_a})/k_BT]\, d\mathbf{r}^{N_a}\, d\omega^{N_a}\right) \\ &= x_\kappa x_\alpha m N_{site}^{top}\int\frac{\partial}{\partial(\sigma_{\kappa\alpha}^3)}\left[\varepsilon_{\kappa\alpha}f\left(\frac{r_{\kappa\alpha}}{\sigma_{\kappa\alpha}}\right)\right] \times \rho(\mathbf{r}_1, \omega_1)\, d\mathbf{r}_1\, d\omega_1 \end{aligned} \quad (8)$$

where $x_\kappa = N_\kappa/(mN_a)$ is the mole fraction of site species κ in adsorbate phase, N_a is the number of adsorbate molecules, and $x_\alpha = N_\alpha/N_{site}^{top}$ is the mole fraction of sites of species α on the top of the rough surface. The one-body density-orientation profile $\rho(\mathbf{r}_1, \omega_1)$ is defined in the grand canonical ensemble as[50]

$$\rho(\mathbf{r}_1, \omega_1) = \frac{1}{\Xi}\sum_{N_a=1}^{\infty}\frac{z_a^{N_a}}{(N_a-1)!}\int \exp(-U/k_BT) \times d\mathbf{r}_2\, d\mathbf{r}_3 ... d\mathbf{r}_{N_a}\, d\omega_2\, d\omega_3 ... d\omega_{N_a} \quad (9)$$

We now take the reference system limit, $\varepsilon_{\kappa\alpha} \to \varepsilon_x$, $\sigma_{\kappa\alpha} \to \sigma_x$, and $q_\alpha \to q_x^+$ (or q_x^-). Equation 8 gives

$$\left(\frac{\partial\Omega}{\partial\sigma_{\kappa\alpha}^3}\right)_x = x_\kappa x_\alpha F_{x,\kappa\alpha} \quad (10)$$

where

$$F_{x,\kappa\alpha} = mN_{site}^{top}\int\frac{\partial}{\partial(\sigma_x^3)}\left[\varepsilon_x f\left(\frac{r_{\kappa\alpha}}{\sigma_x}\right)\right]\rho_x(\mathbf{r}_1, \omega_1)\, d\mathbf{r}_1\, d\omega_1 \quad (11)$$

where $\rho_x(\mathbf{r}_1, \omega_1)$ is the corresponding one-body density-orientation profile in the reference system. Similarly, the derivative with respect to $\varepsilon_{\kappa\alpha}\sigma_{\kappa\alpha}^3$ in eq 7 can be evaluated in the reference system as

$$\left(\frac{\partial\Omega}{\partial(\varepsilon_{\kappa\alpha}\sigma_{\kappa\alpha}^3)}\right)_x = x_\kappa x_\alpha G_{x,\kappa\alpha} \quad (12)$$

where

$$G_{x,\kappa\alpha} = mN_{site}^{top}\int\frac{\partial}{\partial(\varepsilon_x\sigma_x^3)}\left[\varepsilon_x f\left(\frac{r_{\kappa\alpha}}{\sigma_x}\right)\right]\rho_x(\mathbf{r}_1, \omega_1)\, d\mathbf{r}_1\, d\omega_1 \quad (13)$$

Now, we consider the derivatives with respect to q_α in eq 7:

$$\begin{aligned}\frac{\partial\Omega}{\partial(q_\alpha)} &= -k_BT\frac{1}{\Xi}\frac{\partial\Xi}{\partial(q_\alpha)} = -k_BT\frac{1}{\Xi}\left(\sum_{N_a=0}^{\infty}\frac{z_a^{N_a}}{N_a!} \times \int\frac{\partial(-U/k_BT)}{\partial(q_\alpha)}\exp[-U(\mathbf{R}^{\{N_\alpha\}}, \mathbf{r}^{N_a}, \omega^{N_a})/k_BT]\, d\mathbf{r}^{N_a}\, d\omega^{N_a}\right) \\ &\approx \frac{N_\alpha}{\Xi}\left(\sum_{N_a=0}^{\infty}\frac{z_a^{N_a}\sum_\kappa N_\kappa}{N_a!}\int\frac{\partial}{\partial(q_\alpha)}\left[\frac{q_\kappa q_\alpha}{4\pi\varepsilon_0 r_{\kappa\alpha}}\right] \times \exp[-U(\mathbf{R}^{\{N_\alpha\}}, \mathbf{r}^{N_a}, \omega^{N_a})/k_BT]\, d\mathbf{r}^{N_a}\, d\omega^{N_a}\right) \\ &= \frac{1}{4\pi\varepsilon_0}\sum_\kappa x_\kappa x_\alpha q_\kappa m N_{site}^{top}\int\frac{1}{r_{\kappa\alpha}}\rho(\mathbf{r}_1, \omega_1)\, d\mathbf{r}_1\, d\omega_1 \end{aligned} \quad (14)$$

When we take the reference system limit, eq 14 gives

$$\left(\frac{\partial\Omega}{\partial(q_\alpha)}\right)_x = \sum_\kappa x_\kappa x_\alpha q_\kappa H_{x,\kappa\alpha} \quad (15)$$

where

https://dx.doi.org/10.1021/acs.langmuir.9b03633
Langmuir XXXX, XXX, XXX−XXX

$$H_{x,\kappa\alpha} = \frac{mN_{\text{site}}^{\text{top}}}{4\pi\varepsilon_0} \int \frac{1}{r_{\kappa\alpha}} \rho_x(\mathbf{r}_1, \omega_1)\, \mathrm{d}\mathbf{r}_1\, \mathrm{d}\omega_1 \tag{16}$$

It is apparent that coefficients $F_{x,\kappa\alpha}$, $G_{x,\kappa\alpha}$, and $H_{x,\kappa\alpha}$ are dependent on the site species κ and α due to the site-specific distance $r_{\kappa\alpha}$. From eqs 10, 12, and 15, the expansion series of eq 7 can be rewritten as

$$\begin{aligned}\Omega = \Omega_x &+ \sum_{\kappa}^{\dagger}\sum_{\alpha}^{\dagger} x_\kappa x_\alpha F_{x,\kappa\alpha}(\sigma_{\kappa\alpha}^3 - \sigma_x^3) \\ &+ \sum_{\kappa}^{\dagger}\sum_{\alpha}^{\dagger} x_\kappa x_\alpha G_{x,\kappa\alpha}(\varepsilon_{\kappa\alpha}\sigma_{\kappa\alpha}^3 - \varepsilon_x\sigma_x^3) \\ &+ \sum_{\alpha}^{+}\sum_{\kappa} x_\kappa x_\alpha q_\kappa H_{x,\kappa\alpha}(q_\alpha - q_x^+) \\ &+ \sum_{\alpha}^{-}\sum_{\kappa} x_\kappa x_\alpha q_\kappa H_{x,\kappa\alpha}(q_\alpha - q_x^-) \\ &+ \text{second-order terms ...}\end{aligned} \tag{17}$$

So far, we have not specified the values of ε_x, σ_x, q_x^+, and q_x^- in the reference system. The most sensible choice of the reference system is to make the first-order terms in eq 17 vanish.[28,51] The problem, however, immediately follows that the expressions for the potential parameters of the reference system also depend on the coefficients $F_{x,\kappa\alpha}$, $G_{x,\kappa\alpha}$, and $H_{x,\kappa\alpha}$ which are properties of the reference system that has not been specified. Here, we neglect the site dependence of these coefficients, and with this approximation, these coefficients can be taken outside of the summation operators in eq 17. This assumption is generally acceptable and is supported by the calculation of these coefficients (see Appendix A.3) and the molecular simulation results in section 4. By accepting the approximation that the coefficients $F_{x,\kappa\alpha}$, $G_{x,\kappa\alpha}$, and $H_{x,\kappa\alpha}$ are independent of site type $\kappa\alpha$, annulling the first-order terms in eq 17 yields

$$\varepsilon_x = \frac{\sum_{\kappa}^{\dagger}\sum_{\alpha}^{\dagger} x_\kappa x_\alpha \varepsilon_{\kappa\alpha}\sigma_{\kappa\alpha}^3}{\sum_{\kappa}^{\dagger}\sum_{\alpha}^{\dagger} x_\kappa x_\alpha \sigma_{\kappa\alpha}^3} \tag{18}$$

$$\sigma_x = \left(\frac{\sum_{\kappa}^{\dagger}\sum_{\alpha}^{\dagger} x_\kappa x_\alpha \sigma_{\kappa\alpha}^3}{\sum_{\kappa}^{\dagger}\sum_{\alpha}^{\dagger} x_\kappa x_\alpha}\right)^{1/3} \tag{19}$$

$$q_x^+ = \frac{\sum_{\alpha}^{+} x_\alpha q_\alpha}{\sum_{\alpha}^{+} x_\alpha} \tag{20}$$

$$q_x^- = \frac{\sum_{\alpha}^{-} x_\alpha q_\alpha}{\sum_{\alpha}^{-} x_\alpha} \tag{21}$$

By adding eqs 20 and 21 together and noting the electrical neutrality of the real rough surface, we have

$$\sum_{\alpha}^{+} x_\alpha q_x^+ + \sum_{\alpha}^{-} x_\alpha q_x^- = \sum_{\alpha}^{+} x_\alpha q_\alpha + \sum_{\alpha}^{-} x_\alpha q_\alpha = 0 \tag{22}$$

Equation 22 confirms the electrical neutrality of the reference surface. We also note that only the surface charges in the real system will be mapped onto the reference charges, q_x^+ and q_x^-, in the reference system, while the charges on the adsorbate molecules will be kept unperturbed, and the magnitude of these positive and negative reference charges will, in general, be different. Lorentz−Berthelot combining rules[52,53] are used for the cross-term interaction parameters $\varepsilon_{\kappa\alpha}$ and $\sigma_{\kappa\alpha}$: $\varepsilon_{\kappa\alpha} = (\varepsilon_{\kappa\kappa}\varepsilon_{\alpha\alpha})^{1/2}$ and $\sigma_{\kappa\alpha} = (\sigma_{\kappa\kappa} + \sigma_{\alpha\alpha})/2$. Equations 18−21 correctly reproduce the perturbation expansion of the semigrand potential up to the first order, and they are a surface analog of the vdW1 mixing rules. Similarly, the perturbation treatment to the semigrand potential can also be extended to the adsorbate−adsorbate and adsorbate−lower substrate layer interactions. The potential parameters ε_x^{aa} and σ_x^{aa} for the reference adsorbate−adsorbate (aa) site interactions can be obtained by

$$\varepsilon_x^{\text{aa}} = \frac{\sum_{\kappa}^{\dagger}\sum_{\lambda}^{\dagger} x_\kappa x_\lambda \varepsilon_{\kappa\lambda}\sigma_{\kappa\lambda}^3}{\sum_{\kappa}^{\dagger}\sum_{\lambda}^{\dagger} x_\kappa x_\lambda \sigma_{\kappa\lambda}^3} \tag{23}$$

$$\sigma_x^{\text{aa}} = \left(\frac{\sum_{\kappa}^{\dagger}\sum_{\lambda}^{\dagger} x_\kappa x_\lambda \sigma_{\kappa\lambda}^3}{\sum_{\kappa}^{\dagger}\sum_{\lambda}^{\dagger} x_\kappa x_\lambda}\right)^{1/3} \tag{24}$$

where the summation should be carried over all adsorbate−adsorbate site species κ−λ pairs, none of which has zero size parameter. The mixing rules for the reference charge term will be the same as those for the adsorbate−surface version, but now with a summation over adsorbate site types instead of surface site types (see eqs A.30 and A.31). Equations 23 and 24 are essentially the vdW1 mixing rules for nonspherical molecules.

With these choices for the parameters in the reference system, eq 17 becomes to the first order

$$\Omega \approx \Omega_x \tag{25}$$

Equations 18−21 and 25 together constitute a conformal sites theory for adsorbed films on rough surfaces. The derivation given above has the advantage that it can be extended to higher orders and can be used to derive theories for other properties. The second-order expansion term involves integrations over both the pair and three-body correlation functions for the ideal reference surface. In the case of the vdW1 theory for liquid mixtures, the superposition approximation for the three-body correlation function in terms of the pair functions has been found to give satisfactory results for the second-order term.[28]

The examination of eqs 3, 5, and 6 establishes the reduced semigrand potential as a function of several dimensionless parameters

$$\begin{aligned}\Omega^* \approx F_\Omega\Bigg(&P_{\text{bulk}}^*,\ T^*, V^*, \frac{\varepsilon_x}{\varepsilon_x^{\text{aa}}},\ \frac{\sigma_x}{\sigma_x^{\text{aa}}},\ \frac{\varepsilon_x^{\text{lo}}}{\varepsilon_x^{\text{aa}}},\ \frac{\sigma_x^{\text{lo}}}{\sigma_x^{\text{aa}}},\ \frac{q_x^+}{(4\pi\varepsilon_0\varepsilon_x^{\text{aa}}\sigma_x^{\text{aa}})^{1/2}} \\ &,\ \frac{q_x^-}{(4\pi\varepsilon_0\varepsilon_x^{\text{aa}}\sigma_x^{\text{aa}})^{1/2}},\ \chi_{\text{strc}},\ \chi_{\text{ac}}\Bigg)\end{aligned} \tag{26}$$

where $F_\Omega(...)$ is a universal function for the free energy of systems that obey the same corresponding states principle; the reduced semigrand potential is defined as $\Omega^* = \Omega/\varepsilon_x^{\text{aa}}$, reduced bulk pressure is $P_{\text{bulk}}^* = P_{\text{bulk}}(\sigma_x^{\text{aa}})^3/\varepsilon_x^{\text{aa}}$, reduced temperature is $T^* = k_B T/\varepsilon_x^{\text{aa}}$, and reduced total accessible volume is $V^* = V/(\sigma_x^{\text{aa}})^3$. The ratio of the energy parameters, $(\varepsilon_x/\varepsilon_x^{\text{aa}})$, has been considered as a measure of the fluid wetting on the surface.[54] Potential parameters, ε_x^{lo} and σ_x^{lo}, for the reference adsorbate−lower substrate layer interactions can be calculated by applying the same conformal sites mixing rules (eqs 18 and 19), but now with the summation over all lower layer sites (or atoms). In practice, if the ratios $(\varepsilon_x^{\text{lo}}/\varepsilon_x^{\text{aa}})$ for systems obeying the same corresponding states principle are not too different from each

https://dx.doi.org/10.1021/acs.langmuir.9b03633
Langmuir XXXX, XXX, XXX−XXX

other, it could be neglected. For an energetically rough surface with geometrical defects, a dimensionless structure parameter, χ_{strc}, should be included in the equation to characterize the geometrical heterogeneity of the surface. For example, for a flat surface with a circular geometrical defect of size R_c (see section 3.1), this structure parameter can be defined as $\chi_{strc} = R_c/\sigma_x^{aa}$. To describe the intermolecular forces of the adsorbate molecule, a dimensionless variable, χ_{ac}, similar to the Pitzer's acentric factor for bulk fluids,[55] has been introduced; χ_{ac} considers the effect of the substrate. For adsorptions of simple spherical molecules like Ar, CH_4, etc., this acentric factor χ_{ac} can be neglected. Previous molecular simulations[13] and our calculations show that when σ_x and σ_x^{aa} are not too different from each other, the diameter ratio (σ_x/σ_x^{aa}) has only a minor contribution to the properties of adsorbed films. Then, for the adsorption of spherical molecules, which can be described by the dispersion and overlap interactions only, eq 26 can be simplified to

$$\Omega^* \approx F_\Omega\left(P^*_{bulk},\ T^*, V^*, \frac{\varepsilon_x}{\varepsilon_x^{aa}},\ \chi_{strc}\right) \tag{27}$$

Once the semigrand potential (free energy) is known, other properties, for example, enthalpies of adsorption, including the isosteric heat, and phase transition points, such as capillary condensation and freezing, are readily obtained. Specifically, we are interested in the surface excess adsorption. The reduced surface excess adsorption for a specific substrate structure is given by[21,56]

$$\Gamma^* \approx \Gamma_x(\sigma_x^{aa})^2 = \left(\frac{\langle N_a\rangle_x - V\rho_{bulk}}{S}\right)(\sigma_x^{aa})^2 = F_\Gamma\left(P^*_{bulk},\ T^*, \frac{\varepsilon_x}{\varepsilon_x^{aa}},\ \chi_{strc}\right) \tag{28}$$

where $\langle ... \rangle_x$ denotes the ensemble average in the reference system, ρ_{bulk} is the bulk density of adsorbate molecules, and S is the surface area. The surface excess is an intensive property, so volume is no longer a variable in the function. The corresponding states correlation function F_Γ can be determined from experiments or simulations of any spherical adsorbate molecules adsorbing on the specific substrate. Being determined once, the function F_Γ can be used to predict the surface excess adsorption of other kinds of gas following the same corresponding states correlation.

In summary, the perturbation expansion of the semigrand potential [eq 7 or 17] predicts that the real system is equivalent to the reference system when the ratios of potential parameters of surface sites and those of adsorbate sites equal to unity, that is, $\varepsilon_{\alpha\alpha} : \varepsilon_{\beta\beta} : ... = 1$, $\sigma_{\alpha\alpha} : \sigma_{\beta\beta} : ... = 1$, $|q_\alpha| : |q_\beta| : ... = 1$, $\varepsilon_{\kappa\kappa} : \varepsilon_{\lambda\lambda} : ... = 1$, and $\sigma_{\kappa\kappa} : \sigma_{\lambda\lambda} : ... = 1$. When one or more of these parameter ratios are very different from unity, higher-order terms in the expansion will become important, and our first-order conformal sites theory will fail. In the following sections, we use grand canonical Monte Carlo (GCMC) simulations to explore the limits of applicability of our conformal sites theory to the prediction of adsorption isotherms in highly heterogeneous interfacial systems.

3. MODELING AND METHODS

3.1. Modeling of Heterogeneous Surfaces. In principle, the conformal sites theory can be applied to any substrate structure. Here, we adopted a heterogeneous carbon surface model because of the wide interests in the active carbon materials. We modeled the real substrate as a collection of graphene layers with the top layer being an atomically defective one. The top surface layer is composed of carbon atoms and several types of energetic sties serving as the chemical defects on the surface (e.g., hydroxyl groups, carboxyl groups, etc.). These energetic sites are embedded within the top layer and have a deeper energetic well depth than that of the carbon atoms.[7] Wongkoblap and Do[7] investigated the effects of strength and topology of energetic sites on the adsorption of argon in finite carbon slit pores. They studied four topologies of energetic sites on the surface (centered, cornered, shelled, and random topologies) and found that the topology affects the shape of the adsorption isotherm and the phase transition. In this work, we randomly distributed energetic sites on the surface, which represents the most general case in real applications.

In addition to the chemical heterogeneity on the surface, the geometric defects were also allowed for the top layer using the model of Do and Do.[21] For modeling the geometric defects, we randomly selected a carbon atom on the top layer and then removed it and its surrounding atoms within a certain effective defect radius R_c from the selected atom. The removing action was repeated until the percentage of deleted atoms reached the percentage of defects, P_d. More details can be found in ref 21. This nongraphitized carbon surface model has been shown to be very successful in reproducing experimental data of isosteric heat.[21] In all simulations, we chose $R_c = 2.84$ Å and $P_d = 30\%$; an example of the heterogeneous carbon surface structure is shown in Figure 2.

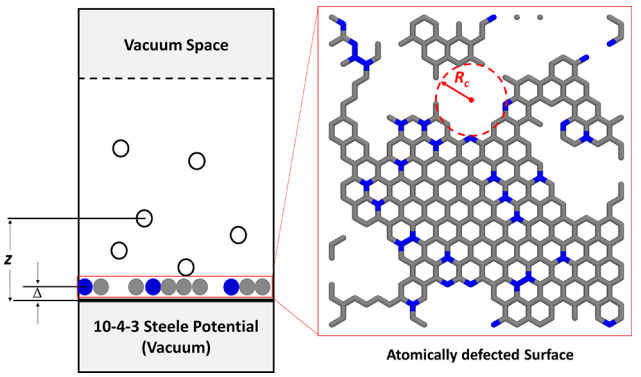

Figure 2. Schematic plot of the simulation box. The top atomically defected layer is composed of carbon atoms (in gray) and 11% energetic sites (in blue), with an effective defect radius of $R_c = 2.84$ Å and a percentage of geometric defects of $P_d = 30\%$. The energetic sites are randomly distributed on the surface. The graphene layers beneath the top defected layer were modeled by the structureless 10-4-3 Steele potential. For the definition of z and Δ, see section 3.2 for details. Adsorbate molecules are shown as white circles.

3.2. Interaction Potentials. To test our conformal sites theory, we ran sets of two parallel GCMC simulations: one for the adsorption on the real surface (cf. the left panel in Figure 1) and the other one for the adsorption on the corresponding ideal reference surface (cf. the right panel in Figure 1). Both real surface and the reference surface share the same structure. For the real system, the potential energy for the site−site interaction between the adsorbate and the top heterogeneous surface was modeled by

https://dx.doi.org/10.1021/acs.langmuir.9b03633
Langmuir XXXX, XXX, XXX−XXX

$$u^{\mathrm{a-top}}(r_{vl}) = 4\varepsilon_{vl}\left[\left(\frac{\sigma_{vl}}{r_{vl}}\right)^{12} - \left(\frac{\sigma_{vl}}{r_{vl}}\right)^{6}\right] + \frac{q_v q_l}{4\pi\varepsilon_0 r_{vl}} \quad (29)$$

where the potential parameters ε_{vl} and σ_{vl} for the interaction between the site v in the adsorbate molecule and the top surface site l were calculated using the Lorentz−Berthelot combining rules. For the reference system, the adsorbate−surface interaction potential was modeled by

$$u_x^{\mathrm{a-top}}(r_{vl}) = 4\varepsilon_x\left[\left(\frac{\sigma_x}{r_{vl}}\right)^{12} - \left(\frac{\sigma_x}{r_{vl}}\right)^{6}\right] + \frac{q_v q_x}{4\pi\varepsilon_0 r_{vl}} \quad (30)$$

where the reference charge q_x denotes either q_x^+ or q_x^-, and the potential parameters ε_x, σ_x, q_x^+, and q_x^- were calculated by the conformal sites mixing rules (eqs 18−21). The adsorbate−adsorbate site−site interaction in the reference system was modeled in the same way as that in the real system (eq 2).

Instead of being simulated explicitly, as for the top surface layer, the graphene layers beneath the top defected layer in both the real system and the reference system were described by the structureless 10-4-3 Steele potential[57]

$$u^{\mathrm{a-lower}}(z) = 2\pi\varepsilon_{\mathrm{as}}\rho_s\sigma_{\mathrm{as}}^2\Delta\left[\frac{2}{5}\left(\frac{\sigma_{\mathrm{as}}}{z}\right)^{10} - \left(\frac{\sigma_{\mathrm{as}}}{z}\right)^{4} - \frac{\sigma_{\mathrm{as}}^4}{3\Delta(z + 0.61\Delta)^3}\right] \quad (31)$$

where z is the distance of adsorbate sites from the graphite surface, ρ_s is the density of the graphite ($\rho_s = 0.114$ Å^{-3}), and Δ is the spacing between two adjacent graphene layers ($\Delta = 3.35$ Å). The adsorbate−graphite energy depth and collision diameter, $\varepsilon_{\mathrm{as}}$ and σ_{as}, were calculated from the Lorentz−Berthelot combining rules. The molecular parameters of the carbon atom in graphite are $\sigma_{ss} = 3.4$ Å and $\varepsilon_{ss}/k_B = 28$ K.[57]

3.3. Choice of Testing Systems. Two general types of system were investigated in this work: a nonpolar system with only site−site Lennard-Jones (LJ) interactions and a polar system with electrostatic interactions.

For the nonpolar system, we studied the adsorption of simple LJ argon on a nongraphitized carbon surface at 87.3 K (normal b.p.). In this case, we assumed that there was only one kind of energetic site (E1) randomly distributed on the top surface, which does not carry any electrostatic charges. Ratios of the LJ energy parameter of the energetic sites (E1) to that of the graphite carbon atom (C), ($\varepsilon_{E1}/\varepsilon_C$), of 1.5, 3.0, and 5.0 and ratios of the LJ size parameters, (σ_{E1}/σ_C), of 1.0, 1.1, and 1.5 were studied. The larger those ratios are, the more likely the reference system would deviate from the real system. When the mole fraction of E1 sites is zero, the energetically heterogeneous surface reduces to an energetically homogeneous surface. We also studied the effect of the mole fraction of energetic sites on the performance of the conformal sites theory. Mole fractions, x_{E1}, of 11.0, 19.9, and 30.2% for the E1 site were tested. Testing systems are summarized in Table 2.

For polar systems where Coulombic forces are involved, we are interested in the adsorption of pure carbon dioxide and pure water vapor on the nongraphitized carbon surface at 273 and 298 K, respectively. We placed four types of energetic polar sites on the top surface: P1, P2, P3, and P4, where P1 and P2 sites carry the positive charges and P3 and P4 carry the negative charges; charge values were chosen in an arbitrary way but were chosen to be of the same order of magnitude as those from the standard force fields. The total mole fraction of these energetic polar sites was kept to about 15% in all cases, which is a reasonable amount for the real rough surface. A good starting point to test the conformal sites theory for polar systems would be to vary the ratios of surface charges, q_{P2}/q_{P1} and q_{P4}/q_{P3}, while keeping the ratios of LJ parameters unity, that is, $\varepsilon_{P1} : \varepsilon_{P2} : \varepsilon_{P3} : \varepsilon_{P4} = 1$ and $\sigma_{P1} : \sigma_{P2} : \sigma_{P3} : \sigma_{P4} = 1$. The CO_2 molecule was represented by three LJ spheres with partial charges centered at each LJ site (TraPPE force field[58]). The C−O bond length and O−C−O bond angle were fixed at the experimental value of 1.16 Å and 180°, respectively. The water molecules were modeled by the simple-point-charge (SPC) water model.[59] Major potential parameters used in the simulation are listed in Table 1, and system parameters for the adsorption of pure CO_2 and water vapor are summarized in Table 3.

Table 1. Major Potential Parameters Used in the Simulation

atom	ε/k_B (K)	σ (Å)	q (e$^-$)
C (graphite)	28	3.4	
LJ argon	119.8	3.405	
C (CO_2)	27	2.8	+0.7
O (CO_2)	79	3.05	−0.35
O (H_2O)	78.197	3.166	−0.82
H (H_2O)			+0.41

Table 2. Systems Tested for LJ Argon Adsorbed on Heterogeneous Surfaces

system no.	σ_{E1}/σ_C	$\varepsilon_{E1}/\varepsilon_C$	x_{E1} (%)
1	1.0	1.5	11.0
2	1.0	3.0	11.0
3	1.0	5.0	11.0
4	1.1	5.0	11.0
5	1.1	5.0	19.9
6	1.1	5.0	30.2
7	1.5	1.5	11.0

For cases studied in Table 2 and Table 3, we compared the adsorption on the real surface and the adsorption on the ideal reference surface side by side to see at which point the reference system will fail to follow the behavior of the real system, where the conformal sites theory breaks down.

3.4. Simulation Details. Grand canonical Monte Carlo (GCMC) simulations were carried out with the Metropolis algorithm.[60] The number and position of substrate sites, chemical potential of adsorbates, accessible volume of the system, and temperature were fixed in the simulation. The box dimension, 31.97 Å × 34.08 Å × 100 Å ($L_x \times L_y \times L_z$), was used to satisfy the periodicity requirement of the graphene structure. The LJ potential cutoff radius was chosen as half of the minimum box length. Three-dimensional periodic boundary conditions were applied. For the calculation of long-range Coulombic interactions, the Ewald summation method was applied.[61,62] An Ewald damping parameter α_E of 0.238 Å^{-1} was used. Following the customary Ewald algorithm, only the central box was accounted for in the real space with a cutoff radius of 15.987 Å. The maximum numbers of k vectors used in the k-space were 10, 10, and 25 in the x, y, and z direction, respectively. The Ewald parameters were selected for best computational efficiency while

https://dx.doi.org/10.1021/acs.langmuir.9b03633
Langmuir XXXX, XXX, XXX−XXX

Table 3. Surface Charges and Mole Fractions Used for CO_2 and H_2O Adsorbed on Heterogeneous Surfaces[a]

system no.	q_{P1} (x_{P1})	q_{P2} (x_{P2})	q_{P3} (x_{P3})	q_{P4} (x_{P4})	q_{P2}/q_{P1} or q_{P4}/q_{P3}
1	+0.4 (0.052)	+0.6 (0.034)	−0.5 (0.052)	−0.75 (0.021)	1.5
2	+0.4 (0.052)	+1.2 (0.034)	−0.5 (0.041)	−1.5 (0.027)	3.0
3	+0.2 (0.034)	+1.0 (0.021)	−0.1 (0.052)	−0.5 (0.045)	5.0
4	+0.1 (0.038)	+1.0 (0.038)	−0.1 (0.038)	−1.0 (0.038)	10.0

[a]LJ potential parameters for all polar energetic sites are set equal to those of the carbon atom in graphite.

ensuring the convergence of the Coulombic energy. We placed an empty vacuum space in the z direction larger than L_x and L_y and applied a correction term for the slab geometry.[63] We explicitly excluded the intramolecular energies of the solid and adsorbate molecules. A schematic plot of the simulation box is shown in Figure 2.

Simulations consisted of 10−40 million moves for equilibrium. The statistics were sampled from the following 10−40 million production moves. The production stage was divided into 100−400 blocks, and the standard error of the mean of these blocks was calculated. Chemical potentials of bulk fluids were obtained either from the Lennard-Jones equation of state[64] or Widom insertion method[65] in isothermal-isobaric (NPT) Monte Carlo simulations.

4. RESULTS AND DISCUSSION

4.1. Ar Adsorption at 87.3 K. In the case of argon adsorption on nongraphitized carbon surfaces, we first test the systems with the LJ size ratio of the energetic surface site (E1) to that of the surface carbon atom (C), (σ_{E1}/σ_C), equal to 1.0, and with the mole fraction of E1, x_{E1}, equal to 11% (Figure 3 a−c). Good overall agreement between the real system and the ideal reference system is seen over the relative pressure range of 1×10^{-5} to 1. The adsorption isotherms in the two different systems are almost identical within the estimated error of simulations. In the low-pressure range from 2×10^{-5} to 1×10^{-4}, however, there are incremental deviations between two systems (see insets in Figure 3 a−c) as the ratio of energy parameters, $(\varepsilon_{E1}/\varepsilon_C)$, increases. The reason for these deviations is that, at a very low pressure, adsorbate molecules will first adsorb on the most active substrate sites on the real surface. However, on the ideal reference surface, all the surface sites are "averaged" to have the same interaction strength with adsorbate molecules; thus, without those active surface sites that are strong enough to attract the adsorbate molecules, the adsorbed amount on the ideal reference surface is expected to be lower at a very low pressure. When the relative pressure goes beyond 1×10^{-4}, the adsorption isotherms of the two systems are in excellent agreement, with the absolute relative deviation within 5%, even as the ratio of LJ energy parameters increases up to 5 (Figure 3c). Furthermore, we notice that the shape of the adsorption isotherm becomes sensitive to the energetic heterogeneities on the real rough surface over the region where the first layer is being completed,[7] which corresponds to the relative pressure range around 2×10^{-4} to 0.1. Therefore, despite the limited performance of the conformal sites theory at relative pressures lower than 1×10^{-4}, which corresponds to the very early stage of the first layer adsorption, the theory can capture the most important part in the adsorption process related to the completion of the monolayer and higher layers and can help us distinguish the strength (or type) of the energetic sites on the surface.

If we increase the LJ size ratio, (σ_{E1}/σ_C), to 1.5 (i.e., volume ratio of 3.375) while keeping the LJ energy parameters ratio,

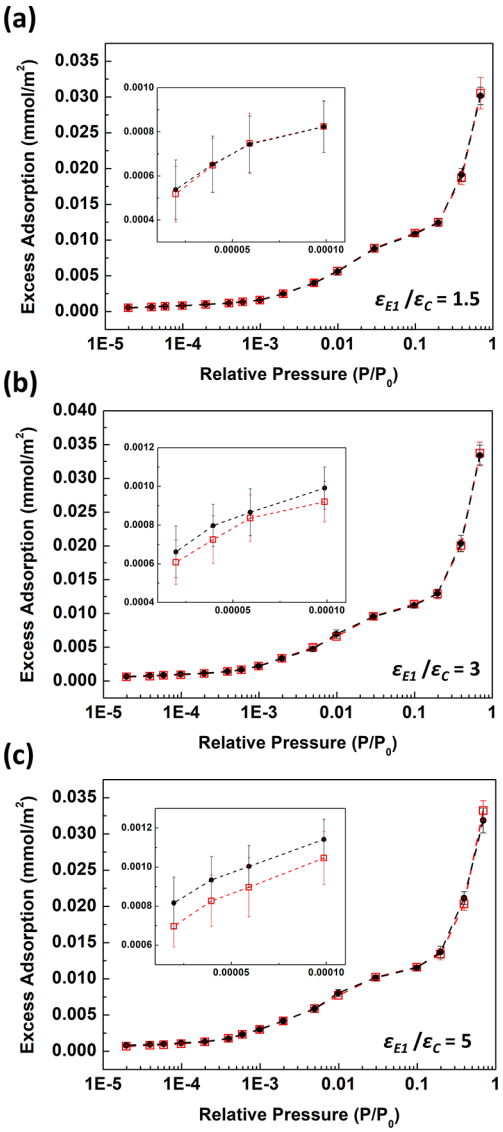

Figure 3. Excess adsorption isotherms of Ar at 87.3 K (normal b.p.) on the real surface (filled black circles) and the ideal reference surface (open red squares) with the LJ size ratio of $\sigma_{E1}/\sigma_C = 1.0$ and $x_{E1} = 11\%$ for the real surface. (a) $\varepsilon_{E1}/\varepsilon_C = 1.5$. (b) $\varepsilon_{E1}/\varepsilon_C = 3$. (c) $\varepsilon_{E1}/\varepsilon_C = 5$. Insets are amplified views of the low-pressure region (relative pressures lower than 0.0001). The saturation pressure, P_0, of argon is 1 atm at 87.3 K. Curves are drawn to guide the eye.

$(\varepsilon_{E1}/\varepsilon_C)$, as low as 1.5, a larger deviation outside the standard errors between the two systems is observed over the monolayer adsorption region, as seen in Figure 4. The reason for the failure is that the conformal sites theory cannot correctly account for the packing effect of the adsorbates on the surface. In the real system (see schematic diagram B in Figure 4), when surface sites differ significantly in size, adsorbates prefer to be irregularly and

https://dx.doi.org/10.1021/acs.langmuir.9b03633
Langmuir XXXX, XXX, XXX−XXX

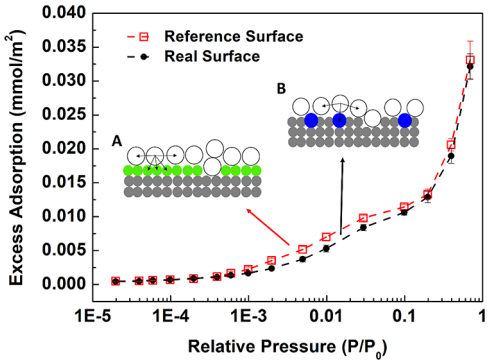

Figure 4. Excess adsorption isotherms of Ar at 87.3 K (normal b.p.) on the real surface and the ideal reference surface with the LJ size ratio of $\sigma_{E1}/\sigma_C = 1.5$, the LJ energy parameters ratio of $\varepsilon_{E1}/\varepsilon_C = 1.5$, and $x_{E1} = 11\%$ for the real surface. The saturation pressure, P_0, of argon is 1 atm at 87.3 K. Curves are drawn to guide the eye. Insets are schematic diagrams of molecular interactions between monolayer adsorbates and surface sites. A: plot for the reference system. B: plot for the real system. The gray circles represent main substrate atoms, green circles represent same-size reference surface sites, blue circles represent large-size energetic sites on the real rough surface, and white circles are adsorbate molecules. See text for details.

loosely packed on the surface, which results in an isotherm that increases more slowly. In the reference system (see schematic diagram A in Figure 4), the size difference of the reference surface sites is smaller, leading to a relatively smooth surface; adsorbate molecules can pack more closely and form a more ordered layer near the surface, favoring the layering transitions.[5,6,21] The sensitivity of the conformal sites theory to the size ratio is expected, and a similar behavior has been observed in the vdW1 theory for hard sphere mixtures at high densities.[46] Georgoulaki et al.[49] concluded that the ratio of the energy parameters influences the performance of the vdW1 theory more than the ratio of the size parameters in binary LJ mixtures. In the interfacial system, however, due to the strong packing effect during adsorption, the ratio of the size parameters of the surface sites is more important than the ratio of the energy parameters. This observation is also supported by the calculation of the coefficient in the perturbation equation (Appendix A.3). If we look at molecular force fields, such as OPLS[36] and TIP,[35] and the force field specifically developed for the functional groups on the surface,[66] the typical LJ energy parameter ratios for the surface sites are within 5.0, and the typical LJ size ratios are within about 1.1. We thus further test the system with $\sigma_{E1}/\sigma_C = 1.1$, $\varepsilon_{E1}/\varepsilon_C = 5$, and mole fractions of $x_{E1} = 11\%$ for the real surface (Figure 5a). The adsorption isotherms from two different systems agree within 5% beyond the low-pressure range ($P/P_0 \geq 2 \times 10^{-4}$).

We have also studied the effect of the mole fraction of surface energetic sites (E1) on the performance of the conformal sites theory. Simulation results are shown in Figure 5. In the low-pressure range ($P/P_0 \leq 1 \times 10^{-4}$), the increase in the mole fraction leads to a growing deviation between the two systems, and the largest relative deviation is up to 25% with respect to the adsorbed amount on the real rough surface. However, at higher pressures, $P/P_0 > 1 \times 10^{-4}$, the simulated adsorption isotherms are within a relative deviation of 5% for the two systems. Thus, other than the low-pressure range, the mole fraction of surface energetic sites, up to 30%, has negligible influence on the performance of the conformal sites theory. It is worth noting that the topology of energetic sites in the current study is limited to

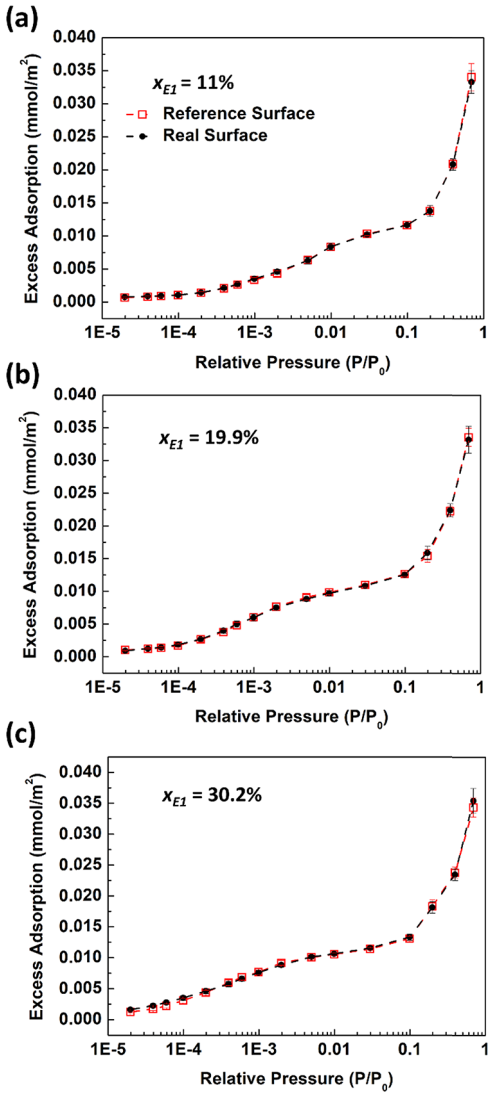

Figure 5. Excess adsorption isotherms of Ar at 87.3 K (normal b.p.) on the real surface (filled black circles) and the ideal reference surface (open red squares) with different mole fractions of energetic sites (E1) on the real surface. (a) $x_{E1} = 11\%$. (b) $x_{E1} = 19.9\%$. (c) $x_{E1} = 30.2\%$. The LJ size ratio is $\sigma_{E1}/\sigma_C = 1.1$, and the LJ energy parameters ratio is $\varepsilon_{E1}/\varepsilon_C = 5$ for all systems. The saturation pressure, P_0, of argon is 1 atm at 87.3 K. Curves are drawn to guide the eye.

the random distribution. We can expect that, for a more locally concentrated site topology, for example, the stripe pattern, the high concentration of the energetic sites would downgrade the applicability of the conformal sites theory more distinctively, especially in the low-pressure region. This is because the more concentrated energetic sites will attract more adsorbate molecules at a low pressure than the random distribution case, resulting in an even larger underestimation of the absorption amount on the ideal reference surface.

In summary, to use the conformal sites theory for the adsorption of simple LJ fluids, we suggest avoiding the low-pressure range, which corresponds to the very early stage of the first-layer adsorption, and also being cautious when applying the conformal sites theory to the system where the surface sites differ largely in size.

4.2. CO_2 Adsorption at 273 K. In this section, we test the conformal sites theory for the adsorption of carbon dioxide with

https://dx.doi.org/10.1021/acs.langmuir.9b03633
Langmuir XXXX, XXX, XXX−XXX

charged polar sites embedded in the heterogeneous surfaces. In this case, the ratio of LJ potential parameters for adsorbate sites is no longer equal to unity. For the TraPPE CO_2 model,[58] the ratio of LJ size parameters is $\sigma_O/\sigma_C \approx 1.089$, and the ratio of LJ energy parameters is $\varepsilon_O/\varepsilon_C \approx 2.9$. In section 4.1, we showed that the conformal sites theory works well when the ratio of size parameters is ~1.1 and the ratio of energy parameters is ~5; based on these results and previous studies,[47−49] we expect that our conformal sites theory should give good results for the contribution of the Lennard-Jones site−site interactions to the CO_2 adsorption.

In Figure 6, we show comparisons for the excess adsorption of CO_2 for the real system and the reference system with different surface charge ratios. We see that, even when the surface charges differ by a factor of 10, the simplified reference system can still reproduce the adsorption behavior of the real system within the estimated errors for most pressure conditions tested. As was the case for argon adsorption, discernible deviations between the real system and the reference system are observed at the low end of the relative pressure range, $P/P_0 < 0.02$. An example is illustrated in Figure 6c with simulation snapshots at $P/P_0 \approx 2.87 \times 10^{-3}$. As highlighted by the black circles, active surface sites strongly attract the adsorbate molecules, and CO_2 molecules accumulate near those sites on the real rough surface. For the ideal reference surface, the surface charges are averaged to have a "mean" value, and those active sites are no longer strong enough to attract CO_2 molecules at low pressures and remain unoccupied.

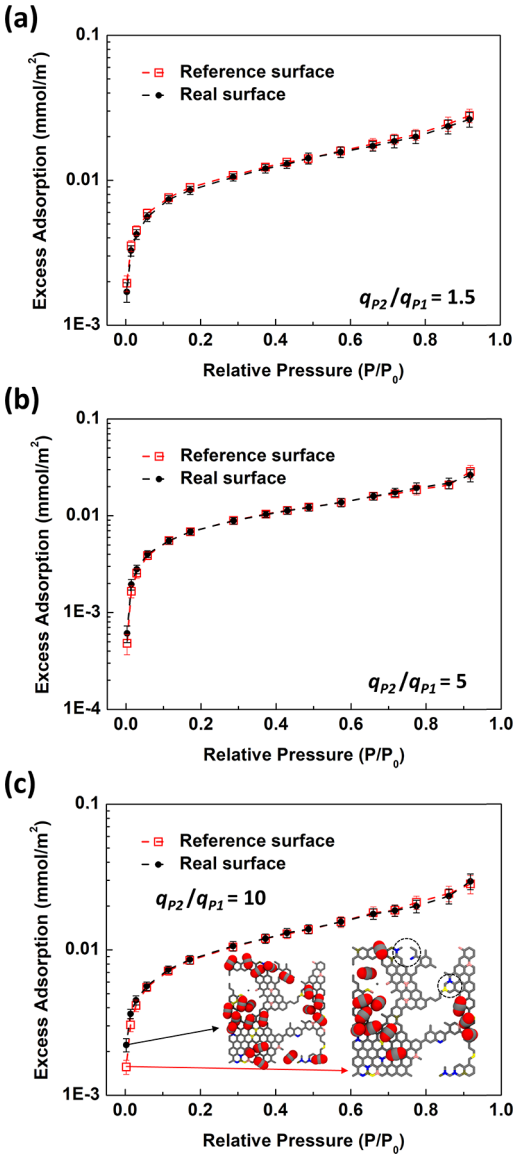

Figure 6. Excess adsorption isotherms of CO_2 at 273 K on the real surface and the ideal reference surface with different surface charge ratios. (a) $q_{P2}/q_{P1} = 1.5$. (b) $q_{P2}/q_{P1} = 5$. (c) $q_{P2}/q_{P1} = 10$. LJ potential parameters for all polar sites are set equal to those of the carbon atoms in graphite, and $q_{P2}/q_{P1} = q_{P4}/q_{P3}$. Detailed system parameters are listed in Tables 1 and 3. The saturation pressure, P_0, of CO_2 is 34.4 atm at 273 K. Insets in (c) are simulation snapshots at $P/P_0 \approx 2.87 \times 10^{-3}$; see text for details. Curves are drawn to guide the eye.

4.3. Water Vapor Adsorption at 298 K. We also investigated the adsorption of water vapor on the heterogeneous carbon surfaces. The major difference between this test and the test with CO_2 is that the H_2O molecules have a large dipole moment and exhibit H-bonding, while the CO_2 molecule has no dipole moment and electrostatic forces are weaker. We show in the following that these differences in the adsorbate interactions have a large impact on the performance of the conformal sites theory and the adsorption mechanism.

The excess adsorption of water vapor on the real rough surface and the ideal reference surface is shown in Figure 7. Unlike the CO_2 case, where the conformal sites theory works even when the charge ratio is as high as 10, here the conformal sites theory deteriorates quickly as the asymmetry of the surface charges increases. When the ratio is 5 (Figure 7c), the reference system deviates from the real system over the full pressure range. The limited success of the conformal sites theory for water vapor adsorption can be attributed to the strong dipole moment and H-bonding of the water molecules. Due to the hydrophobicity of the graphite surface, water molecules will selectively seek polar sites to adsorb. Once the water molecule successfully finds a surface site to occupy, that adsorbed water molecule will serve as a new active sites on the surface, and a 3D cluster or networks will be formed around that surface site through the cooperative bonding effect, involving both fluid−fluid and fluid−energetic site interactions. This adsorption mechanism is clearly shown in the simulation snapshots in Figure 7c; water molecules form a 3D cluster near the strong P2 and P4 polar sites on the real rough surface, while these polar sites are weakened on the reference surface (P2 and P4 sites are marked in the black circle); thus, no water molecules favor them in the reference system.

5. CONCLUSIONS

In this study, we propose a statistical mechanical analysis, which we term conformal sites theory, to account for the chemical heterogeneities of the surface. The theory is also flexible enough to work with a surface with geometric defects. The intermolecular interactions are assumed to consist of a sum of site−site Lennard-Jones interactions plus Coulomb charge−charge terms, a widely used force field for small, relatively rigid molecules and surface sites. The basic assumption of the theory is that all interactions (adsorbate−adsorbate and adsorbate−surface) conform to this same functional form. However, in contrast to early conformal solution theories, our theory takes into account nonspherical molecular shape and distributed charges on the molecules and also can be applied to highly nonuniform systems, such as those experienced in adsorption. We show that the grand potential of the real system with a rough surface can be mapped to that of a system with an ideal reference

https://dx.doi.org/10.1021/acs.langmuir.9b03633
Langmuir XXXX, XXX, XXX−XXX

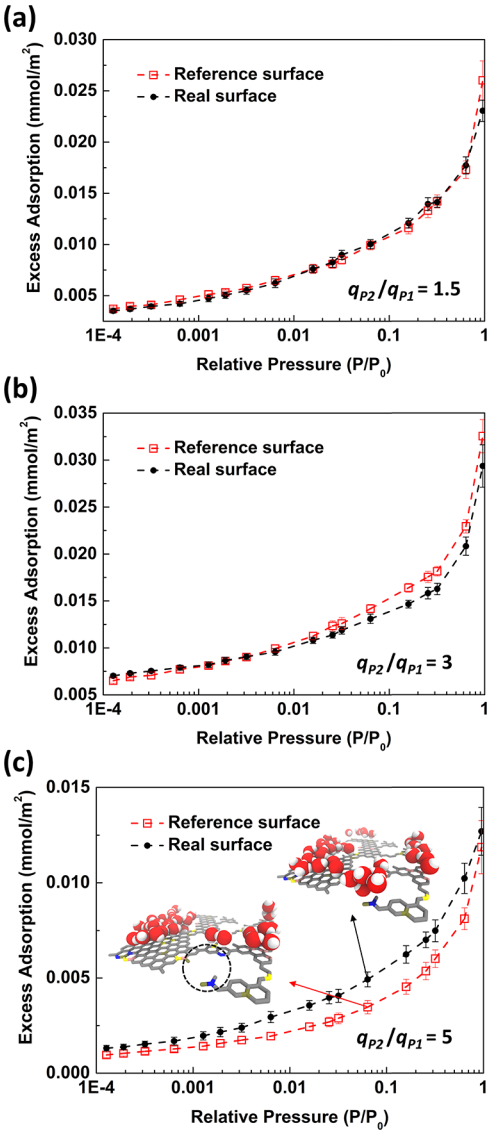

Figure 7. Excess adsorption isotherms of H_2O at 298 K on the real surface and the ideal reference surface with different surface charge ratios. (a) q_{P2}/q_{P1} = 1.5. (b) q_{P2}/q_{P1} = 3. (c) q_{P2}/q_{P1} = 5. LJ potential parameters for all polar sites are set equal to those of the carbon atom in graphite, and $q_{P2}/q_{P1} = q_{P4}/q_{P3}$. Detailed system parameters are listed in Tables 1 and 3. The saturation pressure, P_0, of water is 0.031 atm at 298 K. Insets in (c) are simulation snapshots at $P/P_0 \approx 0.064$; see text for details. Curves are drawn to guide the eye.

surface through a perturbation expansion. Reference surface sites have the same Lennard-Jones (LJ) cross-interaction parameters with the adsorbate sites, and the positively and negatively charged surface sites carry charges q_x^+ and q_x^-, respectively. The first-order perturbation expansion provides mixing rules, eqs 18−21, to calculate the potential parameters for the reference system; these mixing rules, together with eq 25, are the key results of the conformal sites theory for adsorbed films on rough surfaces. The success of the first-order conformal sites theory depends on how different the potential parameters are for the various interactions in the real system; the greater the difference in the potential parameters, the slower will be the convergence of the perturbation expansion so that the first-order theory may not be adequate.

To explore the applicability and limitations of our conformal sites theory, we performed sets of parallel grand canonical Monte Carlo simulations for the real system and the corresponding reference system and compared them side by side to see at which point the adsorption behavior in the reference system starts deviating from that in the real system.

The adsorption of LJ argon at 87.3 K was investigated. We found that the first-order conformal sites theory can give a quantitatively good estimate of the surface excess amount for the adsorption on a highly heterogeneous graphite surface having a single type of embedded energetic site even when the surface atoms (sites) differ in their LJ energy parameters, ε, by a factor of 5, and in the LJ size parameter, σ, by a factor of 1.1. It was also found that the conformal sites theory cannot accurately describe the adsorption in the low-pressure range, where the first few adsorbate molecules seek to occupy the most active surface sites. When the LJ size parameter of the surface sites differs by a large amount, for example, by a factor of 1.5, the conformal sites theory fails to account for the packing effect of adsorbates on the surface, especially during the completion of the monolayer. The effect of the mole fraction of the surface energetic sites was also studied, and it was discovered to have little impact on the performance of the conformal sites theory. In addition, the conformal sites theory was also applied to more complicated systems, where long-range Coulombic interactions are involved. In the case of CO_2 adsorption at 273 K, good agreement between the real system and the corresponding reference system was observed even when the surface energetic sites differ in point charges by a factor of 10, which is larger than the typical value, ∼5, found in commonly used force fields in practice.[66]

Concerning the adsorption of water vapor at 298 K, the performance of the theory deteriorates quickly as the surface polar sites become more asymmetric. The cooperative H-bonding effect during water adsorption magnifies the difference between the real rough surface and the ideal reference surface in terms of the magnitude of electrostatic charges on the surface sites.

In summary, the ratio of LJ size parameters is more important than the ratio of LJ energy parameters for the accuracy of the conformal sites theory. Thus, we suggest exercising caution when applying the theory to an interfacial system where the LJ sites differ greatly in size. The theory should also not be applied at very low pressures if high accuracy is desired. For strongly associating fluids like water, the adsorption is sensitive to the location and electrostatic strength of the polar sites on the surface;[67] in this case, surface point charges of the same sign should not be too different for the theory to work properly. It is worth noting that the performance of conformal sites theory is not monotonically degraded as the increase in the difference of the potential parameters. Due to cancellation of errors, sometimes the theory works unexpectedly well for a more heterogeneous system. Thus, it is not possible to establish a conclusive limit of application of the conformal sites theory, and validation is necessary in some cases. Overall, the current conformal sites theory is good enough for engineering purposes.

Once the conformal sites theory is validated, corresponding states analysis[24] can be performed on the simplified reference system (eqs 26−28), which replaces the corresponding highly heterogeneous real system. Experiments or molecular simulations can then be carried out to establish the corresponding states correlation. Once determined, it could be conveniently used to predict the adsorption properties of other adsorbates (e.g., adsorption isotherms) or to characterize the solid substrate

https://dx.doi.org/10.1021/acs.langmuir.9b03633
Langmuir XXXX, XXX, XXX−XXX

(e.g., geometric roughness using eq 28). Other possible applications of the conformal sites theory include the development of effective solid−fluid interactions for a coarse-grained surface model[14] and the characterization of thin polymer films adsorbed on rough surfaces.[33]

APPENDIX A

A.1. Choice of Expansion Parameters for Lennard-Jones (LJ) Site−Site Terms

We consider a homogeneous fluid in which the N molecules interact with the site−site potential of eq 2, each molecule having m such interaction sites, which can be of species κ, λ... In general, there are N_κ^{intra} sites of species κ within a molecule so that $\sum_\kappa N_\kappa^{\text{intra}} = m$. We label the individual molecules 1, 2, ..., N and the individual intramolecular sites $i\upsilon$, $i\xi$, ... on molecule i. We assume that the intramolecular coordinates of each site are fixed, so the intramolecular energy is excluded in the total configurational internal energy, U_c, which is given, in the canonical ensemble, by

$$\begin{aligned}\langle U_c\rangle &= \frac{1}{2}\sum_{i=1}^{N}\sum_{\substack{j=1\\(i\neq j)}}^{N}\sum_{i\upsilon}\sum_{j\xi}\int\cdots\int u_{i\upsilon j\xi}(r_{i\upsilon j\xi})\\ &\times \frac{\exp[-U(\mathbf{r}^N,\omega^N)/k_BT]}{Z_c}\mathrm{d}\mathbf{r}_1\,\mathrm{d}\mathbf{r}_2\ldots\mathrm{d}\mathbf{r}_N\,\mathrm{d}\omega_1\,\mathrm{d}\omega_2\ldots\mathrm{d}\omega_N\\ &= \frac{N(N-1)}{2}\int\cdots\int u_{12}(r_{12})\,\mathrm{d}\mathbf{r}_1\,\mathrm{d}\mathbf{r}_2\,\mathrm{d}\omega_1\,\mathrm{d}\omega_2\\ &\times \frac{\exp[-U(\mathbf{r}^N,\omega^N)/k_BT]}{Z_c}\mathrm{d}\mathbf{r}_3\ldots\mathrm{d}\mathbf{r}_N\,\mathrm{d}\omega_3\ldots\mathrm{d}\omega_N\\ &= \frac{N(N-1)}{2}\int\cdots\int\sum_{1\upsilon}\sum_{2\xi}u_{1\upsilon2\xi}(r_{1\upsilon2\xi})\,\mathrm{d}\mathbf{r}_1\,\mathrm{d}\mathbf{r}_2\,\mathrm{d}\omega_1\,\mathrm{d}\omega_2\\ &\times \frac{\exp[-U(\mathbf{r}^N,\omega^N)/k_BT]}{Z_c}\mathrm{d}\mathbf{r}_3\ldots\mathrm{d}\mathbf{r}_N\,\mathrm{d}\omega_3\ldots\mathrm{d}\omega_N\\ &= \frac{\rho^2}{2\bar{\omega}^2}\int\cdots\int\sum_{1\upsilon}\sum_{2\xi}u_{1\upsilon2\xi}(r_{1\upsilon2\xi})g(\mathbf{r}_1,\mathbf{r}_2,\omega_1,\omega_2)\\ &\times \mathrm{d}\mathbf{r}_1\,\mathrm{d}\mathbf{r}_2\,\mathrm{d}\omega_1\,\mathrm{d}\omega_2\end{aligned} \tag{A.1}$$

where $\langle\ldots\rangle$ is the ensemble average, $u_{i\upsilon j\xi}$ is the interaction potential for site υ in molecule i and site ξ in molecule j ($i\neq j$); $\rho = N/V$ is the number density of the system; $\bar{\omega} = \int \mathrm{d}\omega$ (4π or $8\pi^2$ for linear or nonlinear molecules, respectively); and $g(\mathbf{r}_1, \mathbf{r}_2, \omega_1, \omega_2)$ is the two-body correlation function given by

$$\begin{aligned}g(\mathbf{r}_1,\mathbf{r}_2,\omega_1,\omega_2) &= \frac{N(N-1)\bar{\omega}^2}{\rho^2}\\ &\times\int\cdots\int\frac{\exp[-U(\mathbf{r}^N,\omega^N)/k_BT]}{Z_c}\mathrm{d}\mathbf{r}_3\ldots\mathrm{d}\mathbf{r}_N\,\mathrm{d}\omega_3\\ &\ldots\mathrm{d}\omega_N\end{aligned} \tag{A.2}$$

Z_c is the configurational partition function of the canonical ensemble

$$\begin{aligned}Z_c &= \int\cdots\int\exp[-U(\mathbf{r}^N,\omega^N)/k_BT]\,\mathrm{d}\mathbf{r}_1\,\mathrm{d}\mathbf{r}_2\ldots\mathrm{d}\mathbf{r}_N\,\mathrm{d}\omega_1\,\mathrm{d}\omega_2\\ &\ldots\mathrm{d}\omega_N\end{aligned} \tag{A.3}$$

We now make an appropriate change of variables[68]

$$\begin{aligned}&g(\mathbf{r}_{12},\omega_1,\omega_2)\mathrm{d}\mathbf{r}_1\mathrm{d}\mathbf{r}_2\mathrm{d}\omega_1\mathrm{d}\omega_2\\ &= g(\mathbf{r}_{1\upsilon2\xi},\omega_1,\omega_2)\mathrm{d}\mathbf{r}_{1\upsilon}\mathrm{d}\mathbf{r}_{2\xi}\mathrm{d}\omega_1\mathrm{d}\omega_2\end{aligned} \tag{A.4}$$

where $\mathbf{r}_{12} = \mathbf{r}_2 - \mathbf{r}_1$ is the intermolecular vector; $\mathbf{r}_{1\upsilon}$ is the position of site υ on molecule 1, site−site separation is $\mathbf{r}_{1\upsilon2\xi} = \mathbf{r}_{2\xi} - \mathbf{r}_{1\upsilon}$. Substituting eq A.4 into eq A.1, integrating over $\mathbf{r}_{1\upsilon}$ and using spherical polar coordinates for $\mathbf{r}_{1\upsilon2\xi}$ gives

$$\begin{aligned}\langle U_c\rangle &= \frac{\rho^2}{2\bar{\omega}^2}\int\cdots\int\sum_{1\upsilon}\sum_{2\xi}u_{1\upsilon2\xi}(r_{1\upsilon2\xi})\\ &\times g(\mathbf{r}_{1\upsilon2\xi},\omega_1,\omega_2)\,\mathrm{d}\mathbf{r}_{1\upsilon}\,\mathrm{d}\mathbf{r}_{2\xi}\,\mathrm{d}\omega_1\,\mathrm{d}\omega_2 = \frac{2\pi N\rho}{\bar{\omega}^2}\\ &\times\int\int\int\sum_{1\upsilon}\sum_{2\xi}u_{1\upsilon2\xi}(r_{1\upsilon2\xi})g(r_{1\upsilon2\xi},\omega_1,\omega_2)\\ &\times r_{1\upsilon2\xi}^2\,\mathrm{d}r_{1\upsilon2\xi}\,\mathrm{d}\omega_1\,\mathrm{d}\omega_2 = 2\pi N\rho m^2\sum_\kappa\sum_\lambda x_\kappa x_\lambda\\ &\times\int_0^\infty u_{\kappa\lambda}(r)g_{\kappa\lambda}(r)r^2\,\mathrm{d}r\end{aligned} \tag{A.5}$$

where, in the last step, due to the integration over the whole space, the site−site distance is independent of the site chosen, that is, $r = r_{1\upsilon2\upsilon} = \ldots = r_{1\xi2\xi}$, and we rewrite the site−site interaction summation between molecule 1 and molecule 2 as the summation of site species κ and λ (on different molecules); $x_\kappa = N_\kappa^{\text{intra}}/m$ is the mole fraction for the site of species κ, and $g_{\kappa\lambda}(r)$ is the site−site correlation function independent of molecular orientations[68]

$$\begin{aligned}g_{\kappa\lambda}(r) &= \langle g(r,\omega_1,\omega_2)\rangle_{\omega_1,\omega_2}\\ &= \frac{1}{\bar{\omega}^2}\int\int g(r,\omega_1,\omega_2)\,\mathrm{d}\omega_1\,\mathrm{d}\omega_2\end{aligned} \tag{A.6}$$

To avoid divergences in the integrals in the derivation that follows, we consider the shielded Coulomb form of eq 2[61,69]

$$u_{\kappa\lambda}(r) = \varepsilon_{\kappa\lambda}f\left(\frac{r}{\sigma_{\kappa\lambda}}\right) + \frac{q_\kappa q_\lambda}{4\pi\varepsilon_0 r}\exp(-br) \tag{A.7}$$

where the constant b is positive but otherwise arbitrary and ensures the convergence of otherwise divergent integrals in what follows. Finally, the limit $b\to 0$ will be taken. Substitution of eq A.7 into eq A.5 and noting that $g_{\kappa\lambda}(r) = h_{\kappa\lambda}(r) + 1$, where $h_{\kappa\lambda}$ is the total correlation function, yields

$$\begin{aligned}\langle U_c\rangle &= 2\pi N\rho m^2\sum_\kappa\sum_\lambda x_\kappa x_\lambda\varepsilon_{\kappa\lambda}\int_0^\infty f\left(\frac{r}{\sigma_{\kappa\lambda}}\right)g_{\kappa\lambda}(r)r^2\,\mathrm{d}r\\ &+ \frac{N\rho m^2}{2\varepsilon_0}\sum_\kappa\sum_\lambda x_\kappa x_\lambda q_\kappa q_\lambda\int_0^\infty\exp(-br)\\ &\times h_{\kappa\lambda}(r)r\,\mathrm{d}r + \frac{N\rho m^2}{2\varepsilon_0}\sum_\kappa\sum_\lambda x_\kappa x_\lambda q_\kappa q_\lambda\\ &\times\int_0^\infty\exp(-br)r\,\mathrm{d}r\end{aligned} \tag{A.8}$$

Electrical neutrality requires that

https://dx.doi.org/10.1021/acs.langmuir.9b03633
Langmuir XXXX, XXX, XXX−XXX

$$\sum_{\kappa} x_\kappa q_\kappa = 0 \tag{A.9}$$

so that the last term in eq A.8 vanishes. Taking the limit $b \to 0$, eq A.8 can be written as

$$\langle U_c \rangle = 2\pi N\rho m^2 \sum_{\kappa}\sum_{\lambda} x_\kappa x_\lambda \varepsilon_{\kappa\lambda} \int_0^\infty f\left(\frac{r}{\sigma_{\kappa\lambda}}\right) g_{\kappa\lambda}(r) r^2 \, dr + \frac{N\rho m^2}{2\varepsilon_0} \sum_{\kappa}\sum_{\lambda} x_\kappa x_\lambda q_\kappa q_\lambda \int_0^\infty h_{\kappa\lambda}(r) r \, dr \tag{A.10}$$

Concerning the second term in eq A.10, we note that, for large r, the interaction will be a dipole−dipole one, and that in this limit the total correlation function approaches zero[70,71] as $h_{\kappa\lambda}(r) \to O(r^{-6})$ so that the integral converges.

Equation A.10 is of multiple site form. We now expand $g_{\kappa\lambda}$ and $h_{\kappa\lambda}$ about the corresponding site−site total correlation functions for a fluid in which all the sites have the same potential energy function, having the form of eq 2 but with parameters ε_x, σ_x, and $\pm q_x$. Retaining only the zeroth order term, eq A.10 can be put in a dimensionless one-site form

$$\langle U_c \rangle_x = 2\pi N\rho m^2 \varepsilon_x {\sigma_x}^3 \int_0^\infty f(r^*) g_x(r^*) (r^*)^2 \, dr^* + \frac{N\rho m^2}{2\varepsilon_0} {q_x}^2 {d_x}^2 \int_0^\infty h_x(r^*) \tilde{r} \, d\tilde{r} \tag{A.11}$$

where subscript x denotes the reference system, and size parameter σ comes out naturally as the length scale to nondimensionalize the variables with respect to the van der Waals interactions, $r^* = r/\sigma_x$ and $\tilde{r} = r/d_x$. Comparing eqs A.10 and A.11, we have

$$\varepsilon_x {\sigma_x}^3 = \sum_{\kappa}\sum_{\lambda} x_\kappa x_\lambda \varepsilon_{\kappa\lambda} {\sigma_{\kappa\lambda}}^3 \tag{A.12}$$

$$q_x^2 d_x^2 = \sum_{\kappa}\sum_{\lambda} x_\kappa x_\lambda q_\kappa q_\lambda {d_{\kappa\lambda}}^2 \tag{A.13}$$

In eqs A.11 and A.13, we have introduced a new length scale, $d_{\kappa\lambda}$ (and d_x), that represents the minimum distance of approach of two point charges, q_κ and q_λ. When the site−site interaction involving these two charges is of the form of eq 2, with both site−site LJ and site−site Coulomb terms, we can take $d_{\kappa\lambda} = \sigma_{\kappa\lambda}$ and $d_x = \sigma_x$, the LJ site−site size parameter. However, some force fields include charge−charge interactions between sites that do not include any LJ term; in these cases, it is helpful to introduce the length parameter $d_{\kappa\lambda}$.

In order to complete the specification of the equivalent reference fluid to which $g_x(r^*)$ refers, we need further expressions for σ_x and d_x or some combination of σ_x (or d_x) and ε_x. We therefore consider a fluid of molecules composed of m hard spheres rigidly joined together, with spheres of species κ, λ... being of diameter $\sigma_{\kappa\kappa}$, $\sigma_{\lambda\lambda}$... Thus the site−site potential is

$$u_{\kappa\lambda}(r) = \infty \quad r \le \sigma_{\kappa\lambda}$$
$$= 0 \quad r > \sigma_{\kappa\lambda} \tag{A.14}$$

where $\sigma_{\kappa\lambda} = (\sigma_{\kappa\kappa} + \sigma_{\lambda\lambda})/2$. The pressure equation for this case is[68]

$$P = \rho kT + \frac{2}{3}\pi m^2 \rho^2 kT \sum_{\kappa}\sum_{\lambda} x_\kappa x_\lambda \sigma_{\kappa\lambda}^2 \langle r_{12} \cos \gamma_{\kappa\lambda} \rangle_{r_{\kappa\lambda}=\sigma_{\kappa\lambda}} \times g_{\kappa\lambda}(\sigma_{\kappa\lambda}^+) \tag{A.15}$$

where $g_{\kappa\lambda}(\sigma_{\kappa\lambda}^+)$ is the value of $g_{\kappa\lambda}(r_{\kappa\lambda})$ at contact, as r approaches $\sigma_{\kappa\lambda}$ from above, and

$$\cos \gamma_{\kappa\lambda} = \hat{\mathbf{r}}_{12} \cdot \hat{\mathbf{r}}_{\kappa\lambda} \tag{A.16}$$

where $\hat{\mathbf{r}}_{12} = \mathbf{r}_{12}/|\mathbf{r}_{12}|$ and $\hat{\mathbf{r}}_{\kappa\lambda} = \mathbf{r}_{\kappa\lambda}/|\mathbf{r}_{\kappa\lambda}|$ are unit vectors along $\mathbf{r}_{12}$ and $\mathbf{r}_{\kappa\lambda}$, respectively, and $\mathbf{r}_{12} = \mathbf{r}_2 - \mathbf{r}_1$ is the line joining the two molecular centers; $\gamma_{\kappa\lambda}$ is the angle between $\mathbf{r}_{12}$ and $\mathbf{r}_{\kappa\lambda}$. In eq A.15, $\langle ... \rangle_{r_{\kappa\lambda}}$ denotes a weighted average over the orientations keeping the site−site distance $r_{\kappa\lambda}$ fixed, that is

$$\langle r_{12} \cos \gamma_{\kappa\lambda} \rangle_{r_{\kappa\lambda}} = \frac{\int\int d\omega_1 \, d\omega_2 \, r_{12} \cos \gamma_{\kappa\lambda} g(\mathbf{r}_{\kappa\lambda}, \omega_1, \omega_2)}{\int\int d\omega_1 \, d\omega_2 \, g(\mathbf{r}_{\kappa\lambda}, \omega_1, \omega_2)} \tag{A.17}$$

Equation A.15 can be put in one-site form by expanding $g_{\kappa\lambda}(\sigma_{\kappa\lambda}^+)$ about $g_x(\sigma_x^+)$ and keeping only terms of zeroth order

$$g_{\kappa\lambda}(\sigma_{\kappa\lambda}^+) = g_x(\sigma_x^+) + ... \tag{A.18}$$

Equation A.15 can then be written in one-site form as

$$P_x = \rho kT + \frac{2}{3}\pi m^2 \rho^2 kT \sigma_x^3 \langle r_{12}^* \cos \gamma_{\kappa\lambda} \rangle_{r_{\kappa\lambda}=\sigma_x} g_x(\sigma_x^+) \tag{A.19}$$

where $r_{12}^* = r_{12}/\sigma_x$ and

$$\sigma_x^3 = \sum_{\kappa}\sum_{\lambda} x_\kappa x_\lambda {\sigma_{\kappa\lambda}}^3 \tag{A.20}$$

Similarly

$$d_x^3 = \sum_{\kappa}\sum_{\lambda} x_\kappa x_\lambda {d_{\kappa\lambda}}^3 \tag{A.21}$$

Equations A.12, A.13, A.20, and A.21 together define the reference fluid, and terms $\varepsilon_x {\sigma_x}^3$ and ${\sigma_x}^3$ come out naturally as the expansion parameters for the LJ site−site terms. However, the current mixing rule for the charge−charge term (eq A.13) suffers from two problems. First, in the cases where LJ size parameters are not available, the optimal choice of the length parameter $d_{\kappa\lambda}$ needs further investigation. Second, in the cases where LJ size parameters are available for the charge sites, eq A.13 becomes

$$q_x^2 \sigma_x^2 = \sum_{\kappa}\sum_{\lambda} x_\kappa x_\lambda q_\kappa q_\lambda {\sigma_{\kappa\lambda}}^2 \tag{A.22}$$

If we assume all interaction sites are of the same size, that is, $\sigma_{\kappa\kappa} = \sigma_{\lambda\lambda} = ... = \sigma_{\kappa\lambda}$, the above equation will reduce to

$$q_x^2 = \sum_{\kappa}\sum_{\lambda} x_\kappa x_\lambda q_\kappa q_\lambda \tag{A.23}$$

Electrical neutrality requires that eq A.9 be obeyed, and we then get $q_x = 0$. This indicates that the conformal sites theory will map a real polar system with partial charges to a reference system without any charge. This unphysical mapping process results from the irrational treatment of the site−site correlation functions for the charge−charge terms. In the next section, we present a new derivation of the mixing rule for the charge term.

A.2. Choice of Expansion Parameters for Electrostatic Term

Here, we consider a homogeneous fluid interacting only with the site−site Coulombic potential. Equation A.10 then leads to

https://dx.doi.org/10.1021/acs.langmuir.9b03633
Langmuir XXXX, XXX, XXX−XXX

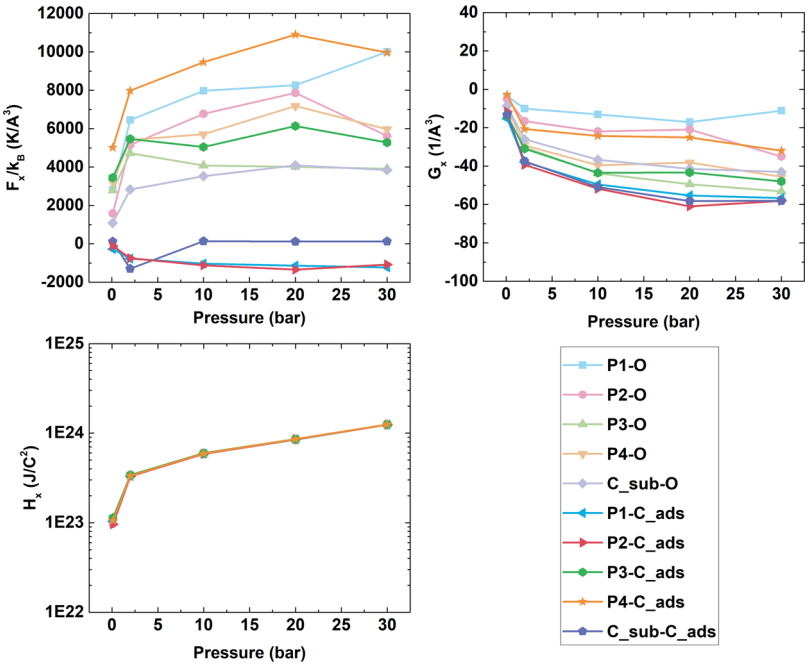

Figure A1. Values of $F_{x,\kappa\alpha}$, $G_{x,\kappa\alpha}$, and $H_{x,\kappa\alpha}$ for different surface (α)−adsorbate (κ) site pairs in system #1 in Table 3 for CO_2 adsorption onto a heterogeneous surface. "O" and "C_ads" denote the oxygen atom and the carbon atom in the CO_2 molecule, respectively. P1, P2, P3, and P4 are energetic polar sites on the surface, and "C_sub" denotes carbon atom in the substrate.

$$\langle U_c \rangle = \frac{N\rho m^2}{2\varepsilon_0} \sum_\kappa \sum_\lambda x_\kappa x_\lambda q_\kappa q_\lambda \int_0^\infty h_{\kappa\lambda}(r) r \, dr \tag{A.24}$$

It is well known that the pair distribution functions for pairs of ions having charges of like sign are significantly different from those for pairs of opposite sign.[72] We therefore divide the summation in eq A.24 into two parts: the summation over site pairs of the same charge sign, and the summation over site pairs of the opposite charge sign. Equation A.24 can then be written as

$$\begin{aligned}\langle U_c \rangle = \frac{N\rho m^2}{2\varepsilon_0} \Bigg(& \sum_\kappa^+ \sum_\lambda^+ x_\kappa x_\lambda q_\kappa q_\lambda \int_0^\infty h_{\kappa\lambda}^+(r) r \, dr \\ & + \sum_\kappa^- \sum_\lambda^- x_\kappa x_\lambda q_\kappa q_\lambda \int_0^\infty h_{\kappa\lambda}^+(r) r \, dr \\ & + \sum_\kappa^+ \sum_\lambda^- x_\kappa x_\lambda q_\kappa q_\lambda \int_0^\infty h_{\kappa\lambda}^-(r) r \, dr \\ & + \sum_\kappa^- \sum_\lambda^+ x_\kappa x_\lambda q_\kappa q_\lambda \int_0^\infty h_{\kappa\lambda}^-(r) r \, dr \Bigg)\end{aligned} \tag{A.25}$$

where $\sum_\kappa^+$and $\sum_\kappa^-$ indicate a summation over all positively charged site types and over all negatively charged site types; $h_{\kappa\lambda}^+$ and $h_{\kappa\lambda}^-$ are the total site−site correlation functions when the two charges are of the same sign and the opposite sign, respectively. We now expand $h_{\kappa\lambda}^+$ and $h_{\kappa\lambda}^-$ about the corresponding reference site−site total correlation functions for a fluid in which all the sites have the same potential energy function but with parameters $q_x^+q_x^+$, $q_x^-q_x^-$, and $q_x^+q_x^-$, where the subscript "x" denotes the reference system; q_x^+ and q_x^- are the reference charge for positively charged sites and negatively charged sites, respectively. Retaining only the zeroth order term, we have

$$h_{\kappa\lambda}^+(r) = h_x^+(r) + \ldots \tag{A.26}$$

$$h_{\kappa\lambda}^-(r) = h_x^-(r) + \ldots \tag{A.27}$$

Substitution of eqs A.26 and A.27 into eq A.25, the total configurational energy can be put into a reference-system form

$$\begin{aligned}\langle U_c \rangle_x = \frac{N\rho m^2}{2\varepsilon_0} \Bigg(& \sum_\kappa^+ \sum_\lambda^+ x_\kappa x_\lambda q_x^+ q_x^+ \int_0^\infty h_x^+(r) r \, dr \\ & + \sum_\kappa^- \sum_\lambda^- x_\kappa x_\lambda q_x^- q_x^- \int_0^\infty h_x^+(r) r \, dr \\ & + \sum_\kappa^+ \sum_\lambda^- x_\kappa x_\lambda q_x^+ q_x^- \int_0^\infty h_x^-(r) r \, dr \\ & + \sum_\kappa^- \sum_\lambda^+ x_\kappa x_\lambda q_x^- q_x^+ \int_0^\infty h_x^-(r) r \, dr \Bigg)\end{aligned} \tag{A.28}$$

By comparing eqs A.25 and A.28 and noting that $\sum_\kappa x_\kappa q_\kappa = 0$ (eq A.9), we obtain

$$\sum_\kappa^+ x_\kappa q_x^+ + \sum_\kappa^- x_\kappa q_x^- = 0 \tag{A.29}$$

$$q_x^+ = \sum_\kappa^+ x_\kappa q_\kappa / \sum_\kappa^+ x_\kappa \tag{A.30}$$

$$q_x^- = \sum_\kappa^- x_\kappa q_\kappa / \sum_\kappa^- x_\kappa \tag{A.31}$$

Equation A.29 imposes the electrical neutrality of the reference system. Equations A.30 and A.31 are the mixing rules for the reference charges, which are just the mole fraction average of the corresponding charges with the same sign on the original fluid molecule.

https://dx.doi.org/10.1021/acs.langmuir.9b03633
Langmuir XXXX, XXX, XXX−XXX

A.3. Calculation of Coefficients $F_{x,k\alpha}$, $G_{x,k\alpha}$, and $H_{x,k\alpha}$ for Different Surface−Adsorbate Site Pairs

If the dispersive and overlap interaction potential is taken to be the 12-6 Lennard-Jones form (see eq 30) and the expansion parameters σ^3 and $\varepsilon\sigma^3$ are treated as two independent variables,[73] eqs 11 and 13 can be rewritten as

$$F_{x,k\alpha} = 4mN_{\text{site}}^{\text{top}}\varepsilon_x{\sigma_x}^3 \int\left[\frac{3{\sigma_x}^6}{{r_{k\alpha}}^{12}} - \frac{1}{{r_{k\alpha}}^6}\right]\rho_x(\mathbf{r}_1, \omega_1)\, \mathrm{d}\mathbf{r}_1\, \mathrm{d}\omega_1 \tag{A.32}$$

$$G_{x,k\alpha} = 4mN_{\text{site}}^{\text{top}} \int\left[\frac{{\sigma_x}^9}{{r_{k\alpha}}^{12}} - \frac{{\sigma_x}^3}{{r_{k\alpha}}^6}\right]\rho_x(\mathbf{r}_1, \omega_1)\, \mathrm{d}\mathbf{r}_1\, \mathrm{d}\omega_1 \tag{A.33}$$

where the site−site distance $r_{k\alpha}$ depends on the molecule position $\mathbf{r}_1$ and orientation ω_1. To illustrate that $F_{x,k\alpha}$, $G_{x,k\alpha}$, and $H_{x,k\alpha}$ can be approximated as site-independent variables, we calculated their values in the case of CO_2 adsorption onto a heterogeneous surface (system #1 in Table 3, where $m = 3$ and $N_{\text{site}}^{\text{top}} = 291$). The one-body density-orientation profile $\rho_x(\mathbf{r}_1, \omega_1)$ in the reference system was evaluated at grid points by uniformly partitioning the simulation box into small cells, and the integration of the profile over the whole space satisfies $\int_V \rho(\mathbf{r}_1, \omega_1)\mathrm{d}\mathbf{r}_1\mathrm{d}\omega_1 = \langle N_a\rangle$, where $\langle N_a\rangle$ is the average number of adsorbate molecules in the system. From Figure A1, we can confirm that $H_{x,k\alpha}$ is site-independent in the full pressure range. While $G_{x,k\alpha}$ shows some site-dependent evidence, the values for different site pairs are still in the same order of magnitude and present a similar trend with increase in the pressure; thus, approximating $G_{x,k\alpha}$ to be site-independent only leads to a small loss of accuracy. The coefficient $F_{x,k\alpha}$, however, shows a stronger dependence on the site pairs than $G_{x,k\alpha}$ and $H_{x,k\alpha}$, indicating that treating $F_{x,k\alpha}$ as a site-independent parameter should be exercised with caution. The behavior of $F_{x,k\alpha}$ further suggests that the success of the conformal sites theory might strongly depend on the difference in the Lennard-Jones (LJ) size parameter, $(\sigma_{k\alpha}^3 - \sigma_x^3)$. If the surface or adsorbate sites differ greatly in size, that is, the difference $(\sigma_{k\alpha}^3 - \sigma_x^3)$ is large, due to the strong site-dependent behavior of $F_{x,k\alpha}$, the first-order term in eq 17 will not be completely annulled by using the conformal sites mixing rules (eqs 18−21), and a non-negligible residual term should be added on the right of eq 25 to make it valid even if the second-order term is still insignificant. In the current CO_2 test case, the first-order term in eq 17 is negligible and is roughly equal to 5×10^{-20} J (0.3 eV) due to small size differences in the adsorbate sites of the CO_2 molecule. The first-order conformal sites theory therefore works well for this system (see Figure 6a).

AUTHOR INFORMATION

Corresponding Authors

Erik E. Santiso − *Department of Chemical & Biomolecular Engineering, North Carolina State University, Raleigh, North Carolina 27606, United States;* orcid.org/0000-0003-1768-8414; Email: eesantis@ncsu.edu

Keith E. Gubbins − *Department of Chemical & Biomolecular Engineering, North Carolina State University, Raleigh, North Carolina 27606, United States;* orcid.org/0000-0001-6760-5897; Email: keg@ncsu.edu

Author

Kaihang Shi − *Department of Chemical & Biomolecular Engineering, North Carolina State University, Raleigh, North Carolina 27606, United States;* orcid.org/0000-0002-0297-1746

Complete contact information is available at: https://pubs.acs.org/10.1021/acs.langmuir.9b03633

Notes

The authors declare no competing financial interest.

ACKNOWLEDGMENTS

The authors thank Yun Long, Qing Shao, and Chongzhi Qiao for helpful discussions. K.S. acknowledges the travel award from the U.S. National Science Foundation under grant no. CBET 1818797 that supports presenting this work at the 8th International Workshop on Characterization of Porous Materials (CPM8), Delray Beach, FL, USA. This work was supported by the National Science Foundation under grant no. CBET 1603851.

REFERENCES

(1) Lastoskie, C.; Gubbins, K. E.; Quirke, N. Pore size heterogeneity and the carbon slit pore: a density functional theory model. *Langmuir* **1993**, *9*, 2693−2702.

(2) Lastoskie, C.; Gubbins, K. E.; Quirke, N. Pore size distribution analysis of microporous carbons: A density functional theory approach. *J. Phys. Chem.* **1993**, *97*, 4786−4796.

(3) Olivier, J. P.; Conklin, W. B.; Szombathely, M. V. Determination of Pore Size Distribution from Density Functional Theory: A Comparison of Nitrogen and Argon Results. *Stud. Surf. Sci. Catal.* **1994**, 81−89.

(4) Olivier, J. P. Modeling physical adsorption on porous and nonporous solids using density functional theory. *J. Porous Mater.* **1995**, *2*, 9−17.

(5) Jagiello, J.; Olivier, J. P. 2D-NLDFT adsorption models for carbon slit-shaped pores with surface energetical heterogeneity and geometrical corrugation. *Carbon* **2013**, *55*, 70−80.

(6) Neimark, A. V.; Lin, Y.; Ravikovitch, P. I.; Thommes, M. Quenched solid density functional theory and pore size analysis of micro-mesoporous carbons. *Carbon* **2009**, *47*, 1617−1628.

(7) Wongkoblap, A.; Do, D. D. The effects of energy sites on adsorption of Lennard−Jones fluids and phase transition in carbon slit pore of finite length a computer simulation study. *J. Colloid Interface Sci.* **2006**, *297*, 1−9.

(8) Long, Y.; Palmer, J. C.; Coasne, B.; Śliwinska-Bartkowiak, M.; Jackson, G.; Müller, E. A.; Gubbins, K. E. On the molecular origin of high-pressure effects in nanoconfinement: The role of surface chemistry and roughness. *J. Chem. Phys.* **2013**, *139*, 144701.

(9) Coasne, B.; Jain, S. K.; Gubbins, K. E. Freezing of Fluids Confined in a Disordered Nanoporous Structure. *Phys. Rev. Lett.* **2006**, *97*, 105702.

(10) Coasne, B.; Jain, S. K.; Naamar, L.; Gubbins, K. E. Freezing of argon in ordered and disordered porous carbon. *Phys. Rev. B* **2007**, *76*, No. 085416.

(11) Coasne, B. Effect of Surface Texture on Freezing in Nanopores: Surface-Induced versus Homogeneous Crystallization. *Langmuir* **2015**, *31*, 2706−2713.

(12) Gelb, L. D.; Gubbins, K. E.; Radhakrishnan, R.; Sliwinska-Bartkowiak, M. Phase separation in confined systems. *Rep. Prog. Phys.* **1999**, *62*, 1573−1659.

(13) Radhakrishnan, R.; Gubbins, K. E.; Sliwinska-Bartkowiak, M. Global phase diagrams for freezing in porous media. *J. Chem. Phys.* **2002**, *116*, 1147−1155.

(14) Shi, K.; Santiso, E. E.; Gubbins, K. E. Bottom-Up Approach to the Coarse-Grained Surface Model: Effective Solid−Fluid Potentials for Adsorption on Heterogeneous Surfaces. *Langmuir* **2019**, *35*, 5975−5986.

(15) Lucena, S. M. P.; Oliveira, J. C. A.; Gonçalves, D. V.; Silvino, P. F. G. Second-generation kernel for characterization of carbonaceous material by adsorption. *Carbon* **2017**, *119*, 378−385.

(16) Nguyen, T. X.; Bhatia, S. K. Characterization of Pore Wall Heterogeneity in Nanoporous Carbons Using Adsorption: the Slit Pore Model Revisited. *J. Phys. Chem. B.* **2004**, *108*, 14032−14042.
(17) Ustinov, E. A.; Do, D. D.; Fenelonov, V. B. Pore size distribution analysis of activated carbons: Application of density functional theory using nongraphitized carbon black as a reference system. *Carbon* **2006**, *44*, 653−663.
(18) Röcken, P.; Somoza, A.; Tarazona, P.; Findenegg, G. Two-stage capillary condensation in pores with structured walls: A nonlocal density functional study. *J. Chem. Phys.* **1998**, *108*, 8689−8697.
(19) Huerta, A.; Pizio, O.; Bryk, P.; Sokołowski, S. Application of the density functional method to study phase transitions in an associating Lennard-Jones fluid adsorbed in energetically heterogeneous slit-like pores. *Mol. Phys.* **2000**, *98*, 1859−1869.
(20) Jagiello, J.; Olivier, J. P. Carbon slit pore model incorporating surface energetical heterogeneity and geometrical corrugation. *Adsorption* **2013**, *19*, 777−783.
(21) Do, D. D.; Do, H. D. Modeling of Adsorption on Nongraphitized Carbon Surface: GCMC Simulation Studies and Comparison with Experimental Data. *J. Phys. Chem. B.* **2006**, *110*, 17531−17538.
(22) Liu, Y.; Wilcox, J. Effects of Surface Heterogeneity on the Adsorption of CO_2 in Microporous Carbons. *Environ. Sci. Technol.* **2012**, *46*, 1940−1947.
(23) Kuchta, B.; Firlej, L.; Marzec, M.; Boulet, P. Microscopic Mechanism of Adsorption in Cylindrical Nanopores with Heterogenous Wall Structure. *Langmuir* **2008**, *24*, 4013−4019.
(24) Myers, A. L.; Prausnitz, J. M. Prediction of the adsorption isotherm by the principle of corresponding states. *Chem. Eng. Sci.* **1965**, *20*, 549−556.
(25) Gubbins, K. E.; Long, Y.; Śliwinska-Bartkowiak, M. Thermodynamics of confined nano-phases. *J. Chem. Thermodyn* **2014**, *74*, 169−183.
(26) Leland, T. W., Jr.; Chappelear, P. S.; Gamson, B. W. Prediction of vapor-liquid equilibria from the corresponding states principle. *AIChE J.* **1962**, *8*, 482−489.
(27) Leland, T. W.; Rowlinson, J. S.; Sather, G. A. Statistical thermodynamics of mixtures of molecules of different sizes. *Trans. Faraday Soc.* **1968**, *64*, 1447.
(28) Smith, W. R. Perturbation theory and one-fluid corresponding states theories for fluid mixtures. *Can. J. Chem. Eng.* **1972**, *50*, 271−274.
(29) Rowlinson, J. S.; Swinton, F. L. The statistical thermodynamics of mixtures. In *Liquids and Liquids Mixtures*; Butterworth-Heinemann: London, 1982; pp. 279−315, DOI: 10.1016/B978-0-408-24193-9.50012-6.
(30) McDonald, I. R. Equilibrium theory of liquid mixtures. In *Statistical Mechanics*; Singer, K., Ed., Vol. *1*, Royal Society of Chemistry: Cambridge, 1973; pp. 134−193, DOI: 10.1039/9781847556929-00134.
(31) Gray, C. G.; Gubbins, K. E.; Joslin, C. G. *Theory of Molecular Fluids*; Volume *2*, Applications, Sec. 7.7.1, Oxford University Press: Oxford, 2011.
(32) Mo, K. C.; Gubbins, K. E.; Jacucci, G.; McDonald, I. R. The radial distribution function in fluid mixtures: Conformal solution theory and molecular dynamics results. *Mol. Phys.* **1974**, *27*, 1173−1183.
(33) An, R.; Huang, L.; Mineart, K. P.; Dong, Y.; Spontak, R. J.; Gubbins, K. E. Adhesion and friction in polymer films on solid substrates: conformal sites analysis and corresponding surface measurements. *Soft Matter* **2017**, *13*, 3492−3505.
(34) Lennard-Jones, J. E. Cohesion. *Proc. Phys. Soc.* **1931**, *43*, 461−482.
(35) Jorgensen, W. L. Quantum and statistical mechanical studies of liquids. 10. Transferable Intermolecular Potential Functions for Water, Alcohols, and Ethers. Application to Liquid Water. *J. Am. Chem. Soc.* **1981**, *103*, 335−340.
(36) Jorgensen, W. L. Optimized intermolecular potential functions for liquid alcohols. *J. Phys. Chem.* **1986**, *90*, 1276−1284.
(37) MacKerell, A. D., Jr.; Bashford, D.; Bellott, M.; Dunbrack, R. L., Jr.; Evanseck, J. D.; Field, M. J.; Fischer, S.; Gao, J.; Guo, H.; Ha, S.; Joseph-McCarthy, D.; Kuchnir, L.; Kuczera, K.; Lau, F. T. K.; Mattos, C.; Michnick, S.; Ngo, T.; Nguyen, D. T.; Prodhom, B.; Reiher, W. E.; Roux, B.; Schlenkrich, M.; Smith, J. C.; Stote, R.; Straub, J.; Watanabe, M.; Wiórkiewicz-Kuczera, J.; Yin, D.; Karplus, M. All-Atom Empirical Potential for Molecular Modeling and Dynamics Studies of Proteins †. *J. Phys. Chem. B.* **1998**, *102*, 3586−3616.
(38) Kofke, D. A.; Glandt, E. D. Nearly monodisperse fluids. I. Monte Carlo simulations of Lennard-Jones particles in a semigrand ensemble. *J. Chem. Phys.* **1987**, *87*, 4881.
(39) Kofke, D. A.; Glandt, E. D. Monte Carlo simulation of multicomponent equilibria in a semigrand canonical ensemble. *Mol. Phys.* **1988**, *64*, 1105−1131.
(40) Hansen, J.-P.; McDonald, I. R. Applications to Soft Matter. In *Theory of Simple Liquids*; 4th ed.; Elsevier: 2013, pp. 511−584, DOI: 10.1016/B978-0-12-387032-2.00012-X.
(41) Gray, C. G.; Gubbins, K. E. *Theory of Molecular Fluids*; Volume *1*, Fundamentals, Secs. 3.3 & 3.5, Oxford University Press: Oxford, 1984.
(42) Longuet-Higgins, H. C. The Statistical Thermodynamics of Multicomponent Systems. *Proc. R. Soc. A* **1951**, *205*, 247−269.
(43) Prigogine, I.; Bellemans, A.; Englert-Chwoles, A. Statistical Thermodynamics of Solutions. *J. Chem. Phys.* **1956**, *24*, 518−527.
(44) Scott, R. L. Corresponding States Treatment of Nonelectrolyte Solutions. *J. Chem. Phys.* **1956**, *25*, 193−205.
(45) Henderson, D.; Leonard, P. J. One- and Two-Fluid van der Waals Theories of Liquid Mixtures, II. 6:12 Molecules. *Proc. Natl. Acad. Sci.* **1971**, *68*, 632−635.
(46) Henderson, D.; Leonard, P. J. One- and Two-Fluid van der Waals Theories of Liquid Mixtures, I. Hard Sphere Mixtures. *Proc. Natl. Acad. Sci.* **1970**, *67*, 1818−1823.
(47) Harismiadis, V. I.; Koutras, N. K.; Tassios, D. P.; Panagiotopoulos, A. Z. How good is conformal solutions theory for phase equilibrium predictions? *Fluid Phase Equilib.* **1991**, *65*, 1−18.
(48) Tsang, P. C.; White, O. N.; Perigard, B. Y.; Vega, L. F.; Panagiotopoulos, A. Z. Phase equilibria in ternary Lennard-Jones systems. *Fluid Phase Equilib.* **1995**, *107*, 31−43.
(49) Georgoulaki, A. M.; Ntouros, L. V.; Tassios, D. P.; Panagiotopoulos, A. Z. Phase equilibria of binary Lennard-Jones mixtures: simulation and van der Waals l-fluid theory. *Fluid Phase Equilib.* **1994**, *100*, 153−170.
(50) Gray, C. G.; Gubbins, K. E.; Joslin, C. G. *Theory of Molecular Fluids*; Volume *2*, Applications, Sec. 8.1, Oxford University Press: Oxford, 2011.
(51) Henderson, D.; Leonard, P. J. Conformal Solution Theory: Hard-Sphere Mixtures. *Proc. Natl. Acad. Sci.* **1971**, *68*, 2354−2356.
(52) Lorentz, H. A. Ueber die Anwendung des Satzes vom Virial in der kinetischen Theorie der Gase. *Ann. Phys.* **1881**, *248*, 127−136.
(53) Berthelot, D. Sur le mélange des gaz. *Compt. Rendus.* **1898**, *126*, 1703−1710.
(54) Kumar, V.; Sridhar, S.; Errington, J. R. Monte Carlo simulation strategies for computing the wetting properties of fluids at geometrically rough surfaces. *J. Chem. Phys.* **2011**, *135*, 184702.
(55) Pitzer, K. S.; Lippmann, D. Z.; Curl, R. F., Jr.; Huggins, C. M.; Petersen, D. E. The Volumetric and Thermodynamic Properties of Fluids. II. Compressibility Factor, Vapor Pressure and Entropy of Vaporization 1. *J. Am. Chem. Soc.* **1955**, *77*, 3433−3440.
(56) Hansen, J.-P.; McDonald, I. R.; Hansen, J.-P.; McDonald, I. R. Chapter 2 − Statistical Mechanics. In *Theory of Simple Liquids*; Academic Press, 2013, pp. 13−59, DOI: 10.1016/B978-0-12-387032-2.00002-7.
(57) Steele, W. A. The physical interaction of gases with crystalline solids. *Surf. Sci.* **1973**, *36*, 317−352.
(58) Potoff, J. J.; Siepmann, J. I. Vapor−liquid equilibria of mixtures containing alkanes, carbon dioxide, and nitrogen. *AIChE J.* **2001**, *47*, 1676−1682.
(59) Berendsen, H.J.C.; Postma, J. P. M.; van Gunsteren, W. F.; Hermans, J. Interaction Models for Water in Relation to Protein Hydration. In *Intermolecular Forces*; Pullman, B., Ed., Springer Netherlands: Dordrecht, 1981, pp. 331−342, DOI: 10.1007/978-94-015-7658-1_21.

https://dx.doi.org/10.1021/acs.langmuir.9b03633
Langmuir XXXX, XXX, XXX−XXX

(60) Frenkel, D.; Smit, B. *Understanding molecular simulation: from algorithms to applications*; 2nd ed., Academic Press: San Diego, 2002.
(61) Ewald, P. P. Die Berechnung optischer und elektrostatischer Gitterpotentiale. *Ann. Phys.* **1921**, *369*, 253−287.
(62) Allen, M.P.; Tildesley, D.J. Sec. 6 Long-range forces. In *Computer Simulation of Liquids*; Second Ed., Oxford University Press, 2017, doi: DOI: 10.1093/oso/9780198803195.003.0006.
(63) Yeh, I.-C.; Berkowitz, M. L. Ewald summation for systems with slab geometry. *J. Chem. Phys.* **1999**, *111*, 3155.
(64) Johnson, J. K.; Zollweg, J. A.; Gubbins, K. E. The Lennard-Jones equation of state revisited. *Mol. Phys.* **2006**, *78*, 591−618.
(65) Widom, B. Some Topics in the Theory of Fluids. *J. Chem. Phys.* **1963**, *39*, 2808−2812.
(66) Tenney, C. M.; Lastoskie, C. M. Molecular simulation of carbon dioxide adsorption in chemically and structurally heterogeneous porous carbons. *Environ. Prog.* **2006**, *25*, 343−354.
(67) Müller, E. A.; Rull, L. F.; Vega, L. F.; Gubbins, K. E. Adsorption of Water on Activated Carbons: A Molecular Simulation Study. *J. Phys. Chem.* **1996**, *100*, 1189−1196.
(68) Gray, C. G.; Gubbins, K. E.; Joslin, C. G. *Theory of Molecular Fluids*; Volume *2*, Applications, Secs. 6.7.2, 6.7.3 and 8.1, Oxford University Press: Oxford, 2011.
(69) Mayer, J. E. The Theory of Ionic Solutions. *J. Chem. Phys.* **1950**, *18*, 1426−1436.
(70) Ho/ye, J. S.; Lebowitz, J. L.; Stell, G. Generalized mean spherical approximations for polar and ionic fluids. *J. Chem. Phys.* **1974**, *61*, 3253−3260.
(71) Ho/ye, J. S.; Stell, G. Dielectric constant in terms of atom−atom correlation functions. *J. Chem. Phys.* **1976**, *65*, 18−22.
(72) Hansen, J.-P.; McDonald, I. R. Ionic Liquids. In: *Theory of Simple Liquids*; Elsevier, 2013, pp. 403−454, DOI: 10.1016/B978-0-12-387032-2.00010-6.
(73) Leonard, P. J.; Henderson, D. Conformal solution theory: generalized theory for pure fluids. *Mol. Phys.* **1972**, *23*, 475−487.

https://dx.doi.org/10.1021/acs.langmuir.9b03633
Langmuir XXXX, XXX, XXX−XXX